PHILOSOPHICAL TRANSACTIONS
OF THE ROYAL SOCIETY A
MATHEMATICAL, PHYSICAL AND ENGINEERING SCIENCES

The energy yield potential of a large tidal stream turbine array in the Alderney Race

Journal:	*Philosophical Transactions A*
Manuscript ID	RSTA-2019-0502.R1
Article Type:	Research
Date Submitted by the Author:	18-Apr-2020
Complete List of Authors:	Coles, Daniel; University of Southampton, Energy and Climate Change Division, Sustainable Energy Research Group, School of Engineering Blunden, Luke; University of Southampton, Energy and Climate Change Division, Sustainable Energy Research Group, School of Engineering Bahaj, AbuBakr; University of Southampton, Energy and Climate Change Division, Sustainable Energy Research Group, School of Engineering
Issue Code (this should have already been entered but please contact the Editorial Office if it is not present):	ALDERNEY
Subject:	Energy < ENGINEERING AND TECHNOLOGY, Ocean engineering < ENGINEERING AND TECHNOLOGY
Keywords:	Alderney Race, tidal stream energy, energy yield, large array, array scale blockage

Author-supplied statements

Relevant information will appear here if provided.

Ethics

Does your article include research that required ethical approval or permits?:
This article does not present research with ethical considerations

Statement (if applicable):
CUST_IF_YES_ETHICS :No data available.

Data

It is a condition of publication that data, code and materials supporting your paper are made publicly available. Does your paper present new data?:
My paper has no data

Statement (if applicable):
CUST_IF_YES_DATA :No data available.

Conflict of interest

I/We declare we have no competing interests

Statement (if applicable):
CUST_STATE_CONFLICT :No data available.

Authors' contributions

This paper has multiple authors and our individual contributions were as below

Statement (if applicable):
Daniel Coles built and validated the hydrodynamic model, ran all model simulations, conducted post processing of computational results and drafted the manuscript. Luke Blunden assisted in the build and validation of the English Channel hydrodynamic model and provided input to the analysis of model results and drafting the manuscript. AbuBakr Bahaj assisted in drafting the manuscript and supervising the research.

PHILOSOPHICAL TRANSACTIONS A

Phil. Trans. R. Soc. A.

doi:10.1098/not yet assigned

The energy yield potential of a large tidal stream turbine array in the Alderney Race

D.S Coles^+*, L.S Blunden^, A.S. Bahaj^

^†Energy and Climate Change Division, Sustainable Energy Research Group, School of Engineering, Faculty of Engineering and Applied Sciences, University of Southampton, Southampton, SO16 7QF, UK
+SIMEC Atlantis Energy, 4th Floor, Edinburgh Quay 2, 139 Fountainbridge, Edinburgh, EH3 9QG, UK

Keywords: Alderney Race, tidal stream energy, energy yield, large array, array scale blockage

Summary

This research provides an updated energy yield assessment for a large tidal stream turbine array in the Alderney Race. The original array energy yield estimate was presented in 2004. Enhancements to this original work are made through the use of a validated 2D hydrodynamic model, enabling the resolution of flow modelling to be improved, whilst also quantifying the impacts of array blockage. Results show that a range of turbine designs (i.e. rotor diameter and power capacity) are needed for large scale development, given the spatial variation in bathymetry and flow across the Alderney Race. Array blockage causes a reduction in flow speeds in the array of up to 2.5 m/s, increased flow speeds around the array of up to 1 m/s and a reduction in the mean volume flux through the Alderney Race of 8%. The annual energy yield estimate of the array is 3.18 TWh, equivalent to the electricity demand of around 1 million homes. The capacity factor of the array is 18%, implying sub-optimal array design. This demonstrates the need for the turbine rated speeds to be selected based on the altered flow regime, not the ambient case. Further enhancement to array performance is explored through increases to rotor diameter and changes to device micro-siting, demonstrating the significant potential for array performance improvement.

1. Introduction

a. Potential for large scale power generation

Tidal flows in the Alderney Race contain a significant energy resource that rivals that of other well-known sites such as the Pentland Firth in Scotland and Minas Passage in Canada (1–3). However, the amount of energy that could practically be harnessed by large tidal stream turbine arrays in the Alderney Race for the purposes of electrical power generation remains unclear. Quantifying this potential for electricity generation

*Author for correspondence (d.coles@soton.ac.uk)

†Present address: Energy and Climate Change Division, Sustainable Energy Research Group, School of Engineering, Faculty of Engineering and Applied Sciences, University of Southampton, Southampton, S016 7QG, UK

not only establishes how tidal stream energy can contribute alongside other generation technologies to meet demand, it is also necessary to understand additional benefits tidal stream energy projects can provide to the region. These include local economic benefits, local job creation and cost reduction through economies of volume, as has been demonstrated for UK sites (4).

Resource assessment studies carried out on the Alderney Race to date offer initial indications of the electrical generation potential of the Alderney Race, providing a basis for further enhancement. However, these estimates contain high levels of uncertainty. This uncertainty manifests as a result of (a) the use of low-resolution bathymetry and flow data, (b) methods for modelling energy extraction that neglect regional and array scale blockage effects, (c) consideration of a wide variety of array configurations, and/or (d) a reliance on idealized geometric and tidal flow modelling (1,5–12). This research aims to address some of these limitations.

Results are presented from a validated 2D hydrodynamic model that simulates energy extraction by a tidal stream turbine array in the Alderney Race. This builds on the work presented in (5), which considered a 3.26 GW array, as described in Section 1b. In this paper the same array design is considered to provide updated energy yield estimates though enhanced modelling capability. The enhancements to array modelling that are presented in this paper are summarised in Table 1. Case 1 is the approach taken in (5) and described in Section 1b. Arrows indicate the data input/modelling approach that changes to go from the previous case to the next. Case 2 provides improvements to the spatial and temporal resolution of bathymetry and flow data from validated 2D hydrodynamic modelling, which is described in Section 2. Ambient flow results from the hydrodynamic model are used to assess the accuracy of the energy yield estimates made in Case 1. Results from this assessment are presented in Section 3a. Case 3 models the added array drag within the hydrodynamic model to quantify the impacts of array scale blockage on energy yield (Section 3b). Cases 4 and 5 explore array performance improvement measures through enhancements to device power coefficient and array capacity (Section 4a-b). Additional array performance improvements to device rotor diameter and device micro-siting are explored in Section 4c-d.

The significance of the assessment provided in (5) was that it was the first peer-reviewed estimate of the tidal energy resource in the Alderney Race published since the resurgence of interest in tidal stream power in the late 1990s. It has been cited over 140 times at the time of writing (January 2020), and provided a nucleus for other resource assessment work around the UK, such as (13,14). It is acknowledged in (5) that there are several

aspects of the work that require further investigation to refine the array energy yield estimate. Firstly, it is unclear if the flow data obtained from Admiralty Charts at relatively low spatial and temporal resolution is representative of the flow speeds at the sub-array locations. Secondly, array scale blockage effects are neglected, but are likely to detrimentally impact upon power performance if flow is re-directed around the sub-arrays as a result of their added drag. Therefore, it is of interest to revisit the estimates in the light of new bathymetric and validation datasets, and improved modelling capabilities.

b. Sub-array modelling in the Alderney Race

The energy produced by seventy eight '1st generation' sub-arrays in the Alderney Race was first estimated in (5). The collection of sub-arrays, which we term the 'array', has a total installed capacity of 3,261 MW. Figure 1 shows the location of the sub-arrays in the Alderney Race. Each sub-array contains sixteen twin rotor devices that are positioned in two rows of eight. The longitudinal spacing between rows is eighteen rotor diameters. The lateral spacing between each device is five rotor diameters. In (5) the hub height, rotor diameter and rated power of the devices in each sub-array were selected based upon the depth and ambient flow speeds at the sub-array locations, using low spatial resolution data from Admiralty Charts. The specifications of the devices are outlined in Table 2. A breakdown of the number of sub-arrays, and their rated capacities is set out in Table 3.

The total installed capacity of the thirty-five 1st generation sub-arrays in the East Race is 2127 MW. Twenty-nine of the thirty-five East Race sub-arrays use devices with 14 m diameter rotors and 3.05 MW rated power. These 'small-rotor' sub-arrays each have a power capacity of 49 MW. Four of the East Race sub-arrays use devices with 19 m diameter rotors and 6.20 MW rated power. These 'intermediate rotor' sub-arrays each have a power capacity of 99 MW. The remaining two East Race sub-arrays use devices with 20.5 m diameter rotors and a rated power of 9.70 MW. These 'large rotor' sub-arrays each have a power capacity of 155 MW. The East Race is relatively shallow, with fast flows exceeding 5 m/s in some regions. For this reason, the East Race has a relatively high proportion of devices with small rotor diameters and high rated power.

The West Race contains forty-three 1st generation sub-arrays, with a total installed capacity of 1134 MW. In comparison to the East Race, the West Race is generally deeper with slower flows. To account for this difference in the tidal energy resource, the West Race uses a higher proportion of intermediate and large rotor

sub-arrays, and sub-arrays containing devices with a lower rated speed and rated power. There are nine small rotor sub-arrays in the West Race. The devices in these small rotor sub-arrays each have a rated power of 0.75 MW, making each sub-array power capacity 12 MW. There are nineteen intermediate rotor sub-arrays in the West Race that use devices with a rated power of 1.5 MW. These intermediate rotor sub-arrays each have an installed capacity of 24 MW. The remaining fifteen West Race sub-arrays use devices with 20.5 m diameter rotors and a rated power of 2.40 MW. These 'large rotor' sub-arrays each have a rated power of 38 MW.

Figure 1 also shows the location of 2nd generation devices, located in deeper waters in the North of the Alderney Race. These 2nd generation sub-arrays were also set out originally in (5), however they were excluded from the energy yield estimate. The energy yield potential of these 2nd generation sub-arrays is investigated in this paper with respect to long-term tidal stream energy development in the Alderney Race.

Figure 1 also shows the location of Race Rocks and the South Banks, both in the West Race. Race Rocks are two tower-like bathymetric features that create a downstream jet in high flows. The Alderney South Banks is a dynamic sandbank that runs parallel with the Alderney coast. The influence of Race Rocks on the flow regime and resulting energy extraction of sub-arrays in close proximity to Race Rocks is discussed in this paper. The research presented here also investigates changes to the flow regime at the South Banks as a result of energy extraction by the sub-arrays.

In (5), flow speed data was obtained from Admiralty tidal stream atlas NP 264 at two locations within the Race, one in the East Race and one in the West Race (15). Data was obtained at hourly intervals over one spring tide and one neap tide, commencing 6 hours before Dover high water and ending 6 hours after Dover high water. Flow speeds were obtained in the week between the spring and neap tide using linear interpolation. The annual flow time series was created from 701 12.5 hour period tidal cycles. This approach neglected the variation in tidal cycle period that can range between 12 hours 20 minutes and 12 hours 50 minutes, and the variation in time between spring and neap tides, which can vary between 6 – 8 days in North-West France. Other harmonic effects that govern the strength of the tides to a small degree such as 18.6 year lunar nodal cycle were also ignored.

In (5), the annual energy yield of the array was estimated using the farm method, which is described in Section 2bi. The power output of devices in the downstream row of each sub-array was assumed to be 5%

lower than the power output of devices in the upstream row to account for wake impingement. It was assumed that the wake of each sub-array fully recovered by the location of the next downstream sub-array, as the longitudinal spacing between sub-arrays is kept to 500 m. Array blockage were not considered. The estimated annual energy yield of the array in (5) is 7.40 TWh, with a capacity factor of 26%. This is broken down into 4.73 TWh produced by the East Race sub-arrays, with a capacity factor of 25%, and 2.67 TWh produced by the West Race sub-arrays, with a capacity factor of 27%.

2. Methods

a. Hydrodynamic model description

Telemac 2D was used to build a 2D hydrodynamic model of the English Channel. An in-depth description of the model, including results from a validation study, were first presented in (1). The model solves the shallow water equations using the finite element method (16). The model is driven by tidal elevation data extracted from the European Shelf 2008 model (17) at three open boundaries located in the Irish Sea, Atlantic Ocean and English Channel. Bathymetry data was obtained from the TCarta dataset (18) which has 90 m spatial resolution for the majority of the English Channel. High resolution (1 m) multi swath bathymetry data was used for a small region off the South coast of Alderney, known as the South Banks. In the far extremities of the domain where the TCarta and multi swath data did not reach, such as the North Sea and Celtic Sea, 900 m resolution bathymetry data from the General Bathymetric Chart of the Oceans (GEBCO) dataset was used (19). The bathymetry was mapped onto an unstructured mesh with 5 km resolution in deep water (>50 m), 1 km around the Channel Islands and 250 m in the Alderney Race. Resolving the mesh to finer resolution resulted in no significant change in ambient flow results, indicating that mesh independence had been achieved.

The model was validated using elevation time series at thirteen ports around the domain, including six ports located within the Channel Islands region. At nine out of thirteen ports, M2 and S2 elevation amplitudes and phases showed agreement with real data within 10% and 10° respectively. This included all six ports around the Channel Islands where the Alderney Race is located. The model was also validated against flow timeseries data from three Acoustic Doppler Current Profiler measurement campaigns in the Alderney Race. Results from the validation study show that at the three locations, all M2 major axis amplitudes lie within 10% of the

measured values. Phases and inclinations also show good agreement, with all results excluding one lying within 15° of their true values (1).

b. Energy extraction

i. Farm method

For Case 2, array energy yield was quantified using the Farm method, the same method used in (5). Ambient depth averaged flow speeds were extracted from the hydrodynamic model at the sub-array locations. The power generated by each sub-array was estimated using;

$$P = \frac{1}{2}\rho U^3 C_p A_s \quad (1)$$

Where ρ is the density of seawater, U is flow speed, C_p is the power coefficient of the devices and A_s is the swept area of the device rotors. The cut-in speed of the devices is 1 m/s. In periods when the flow speed exceeds the rated speed of the devices, the power is capped at the rated power of the device. The rated speeds and rated power of each device is summarised in Table 2.

Given the uncertainty in the nature of the boundary layer profile across the Alderney Race, depth averaged flow speeds were used in Equation 1 to estimate sub-array power. In the case of logarithmic boundary layer flow profiles that are often observed in tidal flows, the flow speed at z/h=0.4 is equal to the depth averaged flow speed, where z is elevation above the seabed and h is depth. In the case of most sub-arrays the hub-heights in Table 2 are approximately equal to z/h=0.4, validating this approach.

To account for wake impingement on downstream turbines, the approach taken in (5) is adopted, where the second row of devices in each sub-array have a reduced power output of 5% relative to the upstream row. This makes it possible to infer how improving the spatial and temporal resolution of the ambient flow data impacts upon energy yield estimate, through comparison with results obtained in (5).

The available power to devices at the 1st and 2nd generation sub-array locations was also estimated. The available power is the total power available through the swept area of the devices, before energy extraction takes place. Only a portion of the available power is extracted by the turbine for the purposes of electricity

generation, which is quantified by the power coefficient. For future-generation devices, the power coefficient may differ as a result of improved blade pitch control strategies and increases to rotor diameter, for example. In addition, devices will cap the power they generate at high flow speeds through power shedding, but it is currently unclear what level the rated speed will be set at for future-generation devices. This is also true of the cut-in speed of the devices. The available power negates the need to make assumptions on the value of power coefficient, rated speed and cut-in speed of the devices. This helps provide a consistent approach for assessing the energy resource at different locations, in the absence of device performance and design information. The available power was calculated using;

$$P_a = \frac{1}{2}\rho U^3 A_s \tag{2}$$

ii. Continuous drag method

In Cases 3-5, energy extraction by each sub-array was modelled using the continuous drag method, which is also known as the distributed drag method (20,21). In this method, a sub-array drag coefficient is added to the existing bed drag coefficient in the momentum equations. The sub-array drag term is applied uniformly over each sub-array plot area to simulate the force exerted on the flow by each sub-array. The sub-array drag coefficient is parameterised using the approach taken in (22,23), where the force exerted on the flow by a sub-array is;

$$F = \frac{1}{2}\rho U^2 C_T A_s \tag{3}$$

Where F is the force exerted on the flow by the sub-array, ρ is the density of seawater, U is the flow speed at the sub-array location, C_T is the thrust coefficient of the turbines in the sub-array, assumed to be equal to 0.8 (24), and A_s is the total swept area of the rotors in each sub-array. The sub-array drag is included in the momentum equations as a stress term;

$$\tau_a = \frac{F}{A_p} = \frac{1}{2}\rho U^2 C_T \lambda \tag{4}$$

where τ_a is the added sub-array stress, A_p is the plan area of the sub-array and λ is the sub-array density;

$$\lambda = \frac{A_S}{A_P} \tag{5}$$

The power generated by each sub-array was estimated using Equation 1. In this work, the added drag of the device support structures has been neglected. This was deemed a suitable approach for this early stage investigation so as not to favour any specific turbine and support structure, for which there is limited data available to parameterise support structure drag.

The validity of the continuous drag method was investigated experimentally in (20). The experiments used a recirculating flume, with arrays of porous fences to simulate the added drag of multiple, uniformly distributed rows of turbines. Load cells measured the thrust of each porous fence. The array drag measured by the load cells was compared to results obtained from the distributed drag method. The validity of the continuous drag method depends on the level of agreement between the depth averaged flow speeds used to parameterise drag in Equations 3 and 4, and the actual flow speeds incident on the devices, or in this case, the fences. The level of wake recovery between fence/device rows is dependent on the longitudinal spacing between rows, and/or the magnitude of the ambient turbulence, which aids mixing between the wakes and the accelerated bypass flow surrounding the wakes. This was also investigated in (25–27), demonstrating that in the case of relatively dense arrays, wake impingement on downstream turbines causes depth averaged flow speeds to overestimate the true flow speeds through the turbine plane. It is shown that this often results in the available array power being overestimated because of the inability of depth averaged models to resolve the flow field within the array in three dimensions. In this paper the longitudinal spacing between rows in each sub-array, and between each sub-array, has been maintained to a level to allow wake recovery (28). When the depth averaged flow speeds used to parameterise sub-array drag in Equation 3 are representative of the flow speeds through the devices at their hub-height, as is reasonably assumed here at this stage of the investigation, the distributed drag method provides an appropriate modelling approach.

3. Array performance assessments

a. Farm method (Case 2)

Figure 2 shows the spatial variation in time averaged ambient flow speed within the Alderney Race, obtained from validated hydrodynamic modelling. Flow speeds are greatest in the shallow regions of the East Race at the location of sub-arrays 62 – 67, where the time averaged flow speed exceeds 2.5 m/s. In the West Race, there

is a region of high flow located in the shallow region between the North tip of Alderney and sub-array 17, in the vicinity of Race Rocks. Flow speeds exceed 2.5 m/s in the north region of the East Race as well, at the location of 2nd generation sub-arrays 79 – 81.

Table 4 presents the Case 2 energy yield estimates obtained using the farm method. For comparison, the energy yield and capacity factor estimates from Case 1 in (5), which also used the farm method, but with lower resolution flow data, are included in parentheses. The Case 2 estimated energy yield of all West Race sub-arrays, of 2.90 TWh, agrees within 9% of the Case 1 estimate in (5). The Case 2 energy yield estimate for all East Race sub-arrays is 3.06 TWh, 35% lower than the Case 1 estimate in (5), of 4.73 TWh. Good agreement between Case 1 and Case 2 in the West Race sub-array's energy yield may be expected, as time averaged ambient flow speeds in the West Race show lower spatial variation, making Admiralty Chart data more likely to be representative of the flow over the West Race region. The level of agreement in estimated energy yield is poorer in the East Race where the spatial variation in flow speed is greater, indicating that the flow speeds obtained from Admiralty Charts in Case 1 (5) are only representative of their local region, resulting in over-estimated flow speeds overall.

The average capacity factors of the East Race sub-arrays are relatively low, averaging between 10% and 19%. This is partly due to the high rated speeds of the devices, relative to the ambient flows at the East Race sub-array locations, preventing many of the sub-arrays from reaching their rated power. The second reason for the sub-arrays achieving low capacity factors is that in many cases, the rotors are undersized. This has been brought to light through the use of improved resolution bathymetry data. These two areas of array power performance improvement are explored further in Section 4.

b. Continuous drag method (Case 3)

Case 2 results presented in Section 3a were obtained by adopting the Farm method, which assumes that the ambient flow is not affected by the presence of the sub-arrays, other than the wake impingement that is limited to the second row of each sub-array. In this section, Case 3 results are presented, which demonstrate the impacts of array blockage on (a) the flow regime and (b) sub-array energy yield estimates.

Figure 3 shows the difference in free surface elevation across in the Alderney Race as a result of the added sub-array drag, which was simulated using the continuous drag method. The free surface elevation difference is plotted at peak spring ebb tide, peak spring flood tide, peak neap ebb tide and peak neap flood tide. A positive difference indicates an increase in free surface elevation as a result of the sub-array drag being added. During peak spring ebb and flood tides, the free surface elevation increases upstream of the sub-arrays by approximately 0.3 m relative to the ambient flow. The area of increased free surface elevation shows greatest spatial coverage during flood tide, when the flow is constrained upstream of the sub-arrays by the French coastline to the East. During peak spring ebb tide, the region of increased free surface elevation is focussed mainly upstream of the East Race sub-arrays. Downstream of the sub-arrays, the free surface elevation decreases relative to the ambient flow by up to 0.2 m. These changes to the ambient flow regime increase the free surface elevation difference across the sub-arrays by around 0.5 m, which increases the hydrostatic force that opposes the added sub-array drag.

Compared to peak spring tides, the change in free surface elevation is significantly reduced during peak neap tides. The reduced neap tide flow speeds reduce the magnitude of the added sub-array drag, limiting any changes to free surface elevation. The spatial coverage over which the free surface elevation changes is also reduced in comparison to peak spring tides. The free surface elevation gain upstream of the sub-arrays during peak neap ebb and flood tides is limited to around 0.05 m in both cases. Downstream of the sub-arrays, the free surface elevation reduction is below 0.05 m in small regions, so that the difference in free surface elevation across the sub-arrays increases by around 0.1 m in comparison with the ambient flow field.

Figure 4 shows the difference between the ambient flow speed and the flow speed when sub-array drag is modelled. The flow speed difference is plotted at peak spring ebb tide, peak spring flood tide, peak neap ebb tide and peak neap flood tide. A positive difference indicates an increase in flow speed as a result of the sub-array drag. The location of the Alderney South Banks, a large sandbank to the south of Alderney is also shown to aid discussion. During peak spring ebb tides, there is a reduction in flow speed through the East and West sub-arrays of up to 2.5 m/s. There are significant increases in flow speed through the flanking channels to the West of the West Race sub-arrays and to the East of the East Race sub-arrays of up to 1 m/s. The increase in flow speed through the central channel, between the East and West Race sub-arrays is more modest, at around 0.75 m/s. This is as a result of mass flow conservation; the central is deeper than the flanks, so the reduction in

volume flux through the sub-arrays is compensated by a more modest increase in flow speed than the flanking channel close to the Alderney and France coastlines.

The level of flow reduction within the sub-arrays, and flow increase in the bypass flow through the East and West Race sub-array indicates sub-optimal device placement, as the available resource is being redirected away from the sub-arrays as a result of blockage. It is possible to mitigate this by moving sub-arrays into the central channel between the East and West sub-arrays to create a fence-like structure of devices orientated perpendicular to the flow direction, as demonstrated in (29). Another approach to reduce blockage and increase energy yield may be, somewhat counter intuitively, to reduce the number of sub-arrays in the East and West Race. This was demonstrated for an array spanning the width of Alderney Race in (1), where once the upper bound limit to energy yield has been reached through the addition on devices, any further devices added to the array reduces energy yield due to excessive blockage. The same result could be achieved by reducing the rated power of the devices, so that during high flow speed periods when array drag is greatest, power is shed by the devices, reducing blockage. This is a strategy commonly implemented in operational projects using variable pitch devices.

During peak spring flood tides the reduction in flow speeds within the East and West Race sub-arrays is more modest, whilst still significant, at around 2 m/s. This is expected as generally ebb tides exhibit the highest flow speeds within the Alderney Race.

In the region of the Alderney South Banks the flow increases by up to 1 m/s during peak spring ebb tides. Increases in flow speed increase the shear stress acting on the South Banks, which may result in changes to the sediment dynamics in the region. The flow speeds in the South Banks region appear to be unaffected during flood tides, as the South Banks is located just upstream of the majority of the West Race sub-arrays during these periods. Suffice to say that results have indicated that careful choice of deployment sites is required to prevent hydrodynamic changes that could have a detrimental impact on sediment transport over the Alderney South Banks. Whilst out of the scope of this work, research has been carried out to quantify the impacts of energy extraction on the Alderney South Banks (30,31) and should continue when considering improvements to the array design.

During peak spring flood and ebb tides, the wake created by the East and West Race sub-arrays extends approximately 15 km downstream. During peak neap flood and ebb tides the sub-array wake wakes extend approximately 9 km downstream.

Figure 5 quantifies the ratio of the time averaged flow speed at each sub-array location to its corresponding time averaged ambient flow speed. Time averaged flow speeds are reduced by at least 20% as a result of the added sub-array drag, however there are a few exceptions. The time averaged flow speed at sub-array 35 shows the greatest reduction, of 45%. Sub-array 35 is a large sub-array located in the West Race, south of Race Rocks. During peak spring ebb tide, the flow speed at sub-array 35 is reduced from 3.9 m/s to 1.7 m/s as a result of the added sub-array drag. During peak spring flood tide the reduction in flow speed at sub-array 35 is more modest, reducing from 2.8 m/s to 1.8 m/s. During ebb tides there are six rows of sub-arrays upstream that divert the flow away from sub-array 35. The level of flow diversion is less during flood tides, when there are three sub-arrays upstream of sub-array 35.

The smallest reduction in time averaged flow speed of 8% is at sub-array 45 in the East Race. During flood tides, sub-array 45 is located in the row furthest upstream, limiting array blockage effects as there are no sub-arrays upstream of it. During ebb tides, there are periods when the accelerated flow through the central channel meanders into sub-array 45, increasing the available power to the sub-array.

Figure 6 shows the flow speed difference across the Alderney Race, averaged over the spring-neap period. The ratio of volume flux (Q) to ambient volume flux (Q_0) through the West flank, West Race sub-arrays, central flank, East Race sub-arrays and east flank are shown. The greatest reduction in volume flux reduction of 22% is seen through the West Race sub-arrays. There is a more modest reduction in time averaged volume flux through the East Race sub-arrays of 12%. Whilst the installed capacity of the East Race is greater than the West Race, the devices in the East Race rarely or never reach their rated speed, limiting their added drag. The added sub-array drag causes a reduction in the total volume flux through the Alderney Race of 8%. This results in increased flow speeds in the regions to the West (known as Casquets) and North of Alderney. The maximum increase in instantaneous flow speeds outside of the Alderney Race is around 0.4 m/s in Casquets. Further investigation into the rated speed of the devices is undertaken in Case 5 (Section 4b).

Table 5 summarises the Case 3 estimated annual energy yield from the East and West Race sub-arrays, obtained using the continuous drag method. Numbers in brackets are the results obtained from Case 2 (Section 3a) from the Farm method. The Case 3 results show a significant reduction in estimated energy yield of 62%, from 5.96 TWh to 2.30 TWh when array drag is modelled. This results in an estimated array capacity factor of just 8%. As highlighted, this reduction in energy yield is as a result of the significant reduction in flow speeds through the East and West Race sub-arrays of up to 2.5 m/s, caused by the added sub-array drag. The practical implications of such low capacity factor performance is explored further in Section 4.

4. Power performance improvement measures

a. Turbine power coefficient (Case 4)

Results from recent power curve testing in industry shows that large tidal stream turbines are capable of operating with a power coefficient of 0.41 (32). This is a 37% increase on the assumed power coefficient used in Cases 1-3, of 0.3. Adopting this improvement in power coefficient from 0.3 to 0.41 increases the annual energy yield of the array from 2.30 TWh (Case 3) to 3.18 TWh (Case 4). The East-Race sub-arrays produce 1.76 TWh, with a capacity factor of 9%, whilst the West Race sub-arrays produce 1.42 TWh, with a capacity factor of 14%. The overall capacity factor of the array from 8% (Case 3) to 11% (Case 4). This assumes that the increase in power coefficient results in no increase in the drag coefficient of the devices. An annual array yield of 3.18 TWh is equivalent to the annual electricity demand of approximately 1 million homes, based on an average annual household demand of 2.90 MWh (33).

b. Turbine rated speed (Case 5)

The variation in flow speeds at each sub-array location is characterised in Figure 7. The minimum, maximum, mean and median flow speeds at each of the sub-array locations are plotted, along with the 25th and 75th percentile flow speeds. The results were obtained using the continuous drag approach to include the effects of array blockage. The rated speed of the devices in each sub-array from Cases 1-4 are also plotted for comparison. In the West Race, the maximum flow speeds at the sub-array locations lie between 2 – 3 m/s. Of all the sub-arrays in the West Race, only three sub-arrays experience flows that exceed the rated speed of the devices. In the East Race, none of the sub-arrays experience flows that exceed the rated speed of their devices.

This result highlights that the rated speed of the devices is far too high for the flow speeds incident on the devices.

Reducing the rated speed of the devices to the maximum flow speeds they experience reduces the overall power capacity of the array from 3.26 GW to 2.04 GW, a reduction of 37%. The installed capacity of the East Race sub-arrays reduces from 2127 MW to 775 MW, whilst the installed capacity of the West Race sub-arrays reduces from 1135 MW to 718 MW. The reason for the greater drop in power capacity of the East Race sub-arrays is that there is a greater difference between their rated speeds and the flow speeds incident on them in the East Race, as illustrated in Figure 7. As a result of this, the improvement in capacity factor is greatest across the East Race sub-arrays, increasing from 9% (Case 4) to 19% (Case 5). The capacity factor of the West Race sub-arrays increases from 14% (Case 4) to 16% (Case 5). The overall capacity factor of the array improves from 11% (Case 4) to 18% (Case 5).

This result implies sub-optimal performance, since the capacity factor of operational arrays such as MeyGen 1A are achieving a much higher capacity factor of around 41% (32). In order to increase capacity factor and minimise the cost of the energy produced by the array, oversizing of generators must be prevented. Typically, the rated speed of tidal stream turbines is set to around 70-80% of the maximum flow speed. When flows exceed the rated speed, the devices use blade pitch control to shed power. This reduces loading on the device, which can reduce device costs. Reducing the rated speed of the devices to levels below the maximum flow speed will also reduce blockage during periods when power is shed, helping to minimise changes to the ambient flow regime.

c. Rotor diameter

In Cases 1-5, it is assumed that a clearance between the sea bed and the bottom of the rotor of 25% of the depth (LAT) prevents the rotor from being positioned in the lowest energy region of the water column close to the sea bed (5). A 7 m clearance between the top of the rotor and the free surface (LAT) helps prevent excessive turbine blade loading, which is more likely to occur when the rotor is close to the free surface, exposed to wave induced orbital motion. This also allows navigation of large vessels with relatively large draft directly above the turbines. Similar clearance constraints are adopted operational arrays, such as at MeyGen Phase 1A (34). When the same assumptions around clearance are adopted as (5), but with higher resolution bathymetry, it is evident that the swept area of many device rotors may be increased.

Results from this rotor diameter analysis are presented in Figure 8, which demonstrates that the rotor diameter of devices in forty-four sub-arrays could be increased and remain within the rotor clearance criteria. Conversely twenty one of the twenty nine small East Race sub-arrays have rotors that are oversized based on the rotor clearance criteria adopted. Nevertheless, by utilizing the maximum allowable rotor diameter for devices in all sub-arrays, the total swept area of the array could increase by 32%, from 1.8×10^4 m^2 to 2.4×10^4 m^2. In extreme cases such as that of sub-array 74 and 77, the potential increase in swept area of devices is over 140%, achieved by increasing rotor diameter from 20.5 m to 32 m. The swept area increase will increase the array drag in periods when the turbine is operating below its rated power capacity, as described by Equation 3, so it will have an impact upon the array blockage. For a device in isolation, the percentage increase in energy yield would be similar to the percentage increase in swept area, since power is proportional to swept area. Estimating the uplift in energy yield of the array as a result of this increase in swept area is out of the scope of this paper, however it is expected to be significant.

The criteria used to derive the maximum allowable rotor diameter is not well established. In (5) and in this paper, it has been stipulated that there must be a clearance between the sea-bed and the bottom of the rotor that is equal to 25% of the depth. This is conservative compared to full-scale tidal stream energy devices currently in operation. For example, the MeyGen Phase 1A turbines have a minimum clearance between the sea-bed and the bottom of the rotors of 4.5 m (34). At MeyGen this is equivalent to the lower 13.6% of the water column, since the turbines are installed in depths of around 33 m (LAT). For this reason, there may be scope to increase the diameter of the rotors in the Alderney sub-arrays beyond the levels considered in this paper, given the precedent that has already been set at MeyGen.

Increasing device rotor diameter can reduce cost of energy by minimising balance of system costs, such as the costs of cabling and foundations. This is an approach that has been taken in the wind industry, where increases in rotor diameter have allowed developers with a lease plot of predefined maximum install capacity to install fewer, larger devices, instead of more, smaller devices. This approach can also reduce installation, maintenance and decommissioning costs per mega-watt of installed capacity by reducing the number of turbines in the array.

Increases in blade length will increase the loads on the turbine. Major components such as the blades, gearboxes and the main bearing must be designed to sustain higher loads and greater levels of fatigue whilst maintaining high levels of device efficiency. This will increase the capital cost per turbine. Increases to blade length also increase the likelihood of cavitation at the blade tips as a result of increased blade tip speed. New blade design and material selection are two areas of blade development that could mitigate against detrimental levels of cavitation. Despite these challenges, increasing device energy yield through increased device scale are expected to reduce balance of plant and capital costs per unit of energy produced, as has been seen in the wind industry (4).

d. Sub-array placement

Mitigating flow speed reduction in the array can also be achieved by moving sub-arrays located in low flow regions. Sub-array 35, located in the West Race, which experiences a 45% reduction in time average flow speed due to blockage relative to ambient flow conditions. Moving sub-arrays into the central channel between the East and West Race sub-arrays to form a fence-like structure orientated perpendicular to the flow direction can help mitigate flow diversion around the sub-arrays, as has been demonstrated from array optimisation work in the Alderney Race (29,35). Moving the West Race sub-arrays towards the East may also reduce changes to the ambient flow regime over the South Banks, whilst also preventing the wake generated by Race Rocks impinging on devices, such as those in sub-arrays 14, 20, 22, 29, 31, 35, 37, 42 and 43.

Figure 9a shows the maximum allowable rotor diameter of devices in the 2nd generation sub-arrays (numbers 79-93), based upon the criteria for clearance above and below the rotor originally adopted in (5). With the exception of sub-arrays 80 and 81, the depth (LAT) at all other 2nd generation locations is adequate to fit rotors that exceed 30 m in diameter.

Figure 9b compares the ambient flow speed characteristics at each of the 2nd generation sub-array locations. Flow speeds are greatest at the East Race sub-array locations, where maximum flow speeds of up to 4.9 m/s are observed at sub-array 81. The resource at the West Race sub-arrays appears to be significantly lower, with median flow speeds only just exceeding 1 m/s.

Figure 10 compares the time averaged available power at each of the 1st and 2nd generation sub-array locations, based on the ambient flow field. In general, the available power at the small-rotor West Race sub-array locations is greater than that at the small-rotor East Race sub-arrays. This is because the increase in rotor diameter that is possible in the West Race outweighs the higher ambient flow speeds that are observed in the East Race. This finding is common at other sites, such as those in the Irish Sea where deeper, slower flow regions have a superior potential resource (36). The difference in available power at the intermediate-rotor East and West Race sub-arrays is less obvious, with both sides ranging between 1 – 3 MW. At the large-rotor sub-array locations there appears to be a higher level of available power at the East Race sub-arrays, however there are only two to compare. The available power at the 2nd generation sub-array locations is highest in the East Race, with a maximum level of over 6 MW at sub-array 79. The level of power that can be generated at the sub-array locations will depend upon the device rated power and rotor diameter, and the level of blockage and wake impingement from surrounding devices.

e. Summary of results

Figure 11 summarises the modelling approach taken by the 5 array energy yield assessment cases considered in this paper, as well as the estimated annual energy yield and capacity factor of each case. Case 1 is the approach taken in (5), whilst Cases 2 -5 are the new estimates provided in this paper. The arrows between each case highlights the data input/modelling approach that was modified to provide improved realism from the previous case to the next.

Case 2 improved upon the spatial and temporal resolution bathymetry and flow data relative to Case 1. This was achieved using a validated 2D hydrodynamic model. In Cases 1 and 2 array blockage was excluded. This highlighted that Case 1 overestimated the resource in the East Race where the greatest spatial variations in bathymetry and flow speed were observed. The improved flow characterisation in Case 2 led to a 19% reduction in estimated annual energy yield of the array. Case 3 provided further enhancement through the consideration of array scale blockage, modelled within the hydrodynamic model. Blockage causes reductions in flow speeds of up to 2.5 m/s at the sub-array locations, reducing the estimated array annual energy yield by 61% from Case 2. Case 4 updated the power coefficient of the devices from 0.3 to 0.41, based on recent reported data from full scale operational turbines in industry (32). This increased the estimated annual energy yield obtained in Case 3 by 37%, to 3.18 TWh. Finally, Case 5 reduced the array capacity of the array to

account for the fact that the devices rated speed, and hence rated power, were too high for the flow speeds incident on the devices. Whilst this has no impact on the estimated energy yield of the array, it increases the capacity factor by 63%, from 11% to 18%.

Additional array performance improvements have also been identified. The adoption of higher resolution bathymetry data illustrates that there is potential for the rotor diameter of most devices to be increased, whilst keeping conservative levels of clearance above and below the rotors. This could increase the total swept area of the array by up to 32%. In some cases, the swept area of individual devices have the potential to be increased by over 140%. For an isolated device, this increase in swept area would result in a similar increase in energy yield. Further work is needed to establish how the added drag from swept area increases impacts on the surrounding flow field, and the resulting energy yield. The dependency of energy yield on sub-array location within a spatially variable domain was explored in Section 4d, highlighting the significant increase in the available power to 2nd generation devices relative to 1st generation devices as a result of increases to allowable rotor diameter.

The adoption of the continuous drag method in Cases 3 - 5 highlights that blockage has a significant impact on the surrounding flow regime, impacting on the energy yield of the array. Further work is required to establish the optimal placement of devices within the Alderney Race, with consideration for both energy yield and environmental impacts, such as that on the Alderney South Banks. Progress has been made to optimise device placement and design through the implementation of gradient-based optimisation algorithms, which importantly, accounts for the effects of devices on the flow at each iteration of the optimisation. This has been shown to increase the energy yield of a regular array layout by up to 76% (37). There is therefore scope to build on the work in (29) to apply these optimisation routines within the Alderney Race to further improve array performance.

5. Conclusions

Results from a validated 2D hydrodynamic model are presented to provide an updated energy yield estimate for a large tidal stream turbine array in the Alderney Race. The updated annual energy yield estimate of the array is 3.18 TWh. This updated energy yield estimate is 57% lower than the original estimate presented in (5). This is partly due to improvements made to the resolution of flow data across the Alderney Race, obtained

from the hydrodynamic model. The reduction in estimated energy yield is also caused by the impact of array blockage, which reduces flow speeds within the array by up to 2.5 m/s. Changes to the ambient flow regime caused by array blockage indicate the need for device rated speed to be selected based on the altered flow state (i.e. not the ambient flow regime). This can help reduce the cost of energy by preventing turbines from being over engineered.

Whilst this research indicates that the array design is sub-optimal, measures to improve array performance have been identified. High-resolution bathymetry data shows that the rotor swept area of most devices can be increased whilst maintaining conservative clearance limits above and below each rotor. For some devices this allows rotor swept area to be increased by over 140%. The increase in the total swept area of the array is 32%. Additional array design improvements can be made through modification of sub-array siting. For example, results show that the flow speeds in the channel between the East and West Race sub-arrays increases by up to 0.75 m/s as a result of array blockage, which redirects flow away from the array. Moving West Race sub-arrays into the central channel can help mitigate this re-distribution of the energy resource away from the array. This may also limit changes to the ambient flow regime around the Alderney South Banks, where flow speeds are shown to increase by up to 1 m/s as a result of array blockage. Further study is needed to confirm this. Finally, analysis of the ambient flow regime shows that the available power of the 1st generation devices ranges between 0.5 – 4.5 MW, whilst the available power at the deeper, 2nd generation device locations can exceed 6 MW. This supports the conclusion that through further optimal device siting, the array performance can be improved significantly.

6. Acknowledgements

This work is part of the activities of the Energy and Climate Change Division and the Sustainable Energy Research Group in the Faculty of Engineering and Environment at the University of Southampton (www.energy.soton.ac.uk), UK. It is also supported by grants including the International Centre for Infrastructure Futures (ICIF) (EP/K012347/1), British Council UK Newton Fund (NF) Institutional Links (Grant No. 261850721) and Fortis Unum: Clustering Mini-Grid Networks to Widen Energy Access and Enhance Utility Network Resilience (EP/R030391/1).

7. Contributions

Daniel Coles built and validated the hydrodynamic model, ran all model simulations, conducted post processing of computational results and drafted the manuscript. Luke Blunden assisted in the build and validation of the English Channel hydrodynamic model and provided input to the analysis of model results and drafting the manuscript. AbuBakr Bahaj assisted in drafting the manuscript and supervising the research.

8. References

1. Coles D., Blunden L., Bahaj A. Assessment of the energy extraction potential at tidal sites around the Channel Islands. Energy. 2017;124:171–86.
2. Draper S, Adcock T, Borthwick A, Houslby G. Estimate of the tidal stream power resource of the Pentland Firth. Renew Energy. 63:650–7.
3. Karsten R, McMillan J, Lickley M, Haynes R. Assessment of tidal current energy in the Minas Passage, Bay of Fundy. Proc Inst Mech Eng Part A J Power Energy. 2008;222(5):493–507.
4. Offshore Renewable Energy Catapult. Tidal stream and wave energy cost reduction and industrial benefit. 2018.
5. Bahaj A., Myers L. Analytical estimates of the energy yield potential from the Alderney Race (Channel Islands) using marine current energy converters. Renew Energy. 2004;29(12):1931–45.
6. European Commission. The Exploitation of Tidal and Marine Currents: Non-nuclear Energy JOULE II ; Wave Energy Project Results. 1996.
7. Harwell Laboratory. Energy Technology Support Unit. Tidal stream energy review. 1993.
8. Environmental Change Institute. Variability of UK marine resources. 2005.
9. Myers L, Bahaj A. Simulated electrical power potential harnessed by marine current turbine arrays in the Alderney Race. Renew Energy. 2005;30(11):1713–31.
10. Black and Veatch. Phase II UK tidal stream energy resource assessment. 2005.
11. Black and Veatch. UK tidal current resource and economics. 2011.
12. Blunden L., Bahaj A. Tidal energy resource assessment for tidal stream generators. Proc teh Inst Mech Eng Part A J Power Energy. 2007;221(2):137–46.
13. Blunden L., Bahaj A. Initial evaluation of tidal stream energy resources at Portland Bill, UK. Renew Energy. 2006;31(2):121–32.
14. Lewis M, Neill S, Robins P, Hashemi M. Resource assessment for future generations of tidal-stream

energy arrays. Energy. 2015;83:403–15.

15. Admiralty Charts and Publications. Admiralty sailing directions Channel Pilot, NP 27. 1999.
16. Hervouet J-M. Hydrodynamics of free surface flows modelling with the finite element method. John Wiley & Sons, Ltd; 2007. 24–80 p.
17. Egbert G, Erofeeva S, Ray R. Assimilation of altimetry data for nonlinear shallow-water tides: Quarter-diurnal tides of the Northwest European Shelf. Cont Shelf Res. 2010;30(6):668–79.
18. TCarta. TCarta [Internet]. [cited 2014 Jun 7]. Available from: https://www.tcarta.com/
19. Kapoor D. Technical Note: General bathymetric chart of the oceans (GEBCO). Mar Geod. 1981;5:73–80.
20. Coles D., Blunden L., Bahaj A. Experimental validation of the distributed drag method for simulating large marine current turbine arrays using porous fences. Internatinal J Mar Energy. 2016;16:298–316.
21. Funke S, Kramer S, Piggott M. Design optimisation and resource assessment for tidal-stream renewable energy farms using a new continuous turbine approach. Renew Energy. 2016;99:1046–61.
22. Plew D, Stevens C. Numerical modelling of the effect of turbines on currents in a tidal channel – Tory Channel, New Zealand. Renew Energy. 2013;57:269–82.
23. Walters R, Tarbotton M, Hiles C. Estimation of tidal power potential. Renew Energy. 2013;51:255–62.
24. Bahaj A., Molland J, Chaplin J, Batten W. Power and thrust measurements of marine current turbines under various hydrodynamic flow conditions in a cavitation tunnel and a towing tank. Renew Energy. 2007;32(3):407–26.
25. Vogel C, Willden R, Houlsby G. Power available from a depth-averaged simulation of a tidal turbine array. Renew Energy. 2017;114(B):513–24.
26. Goward Brown A, Neill S, Lewis. Tidal energy extraction in three-dimensional ocean models. Renew Energy. 2017;114(A):244–57.
27. Waldman S, Yamaguchi S, Murray O, Woolf D. Tidal resource and interactions between multiple channels inthe Goto Islands, Japan. Int J Mar Energy. 2017;19:332–44.
28. European Marine Energy Centre Ltd. Assessment of tidal energy resource. 2009.
29. Coles D., Kramer S, Piggott M, Avdis A, Angeloudis A. Optimisation of tidal stream turbine arrays within the Alderney Race. In: The 12th European Wave and Tidal Energy Conference. Cork; 2017.
30. Blunden L., Haynes S, Bahaj A. Tidal current power effects on nearby sandbanks: a case study in the Race of Alderney. Phil Trans Roy Soc A. 2020;In review.
31. Neill S, Jordan J, Couch S. Impact of tidal energy converter (TEC) arrays on the dynamics of headland

sand banks. Renew Energy. 2012;37:3873–97.

32. MeyGen Ltd. Lessons Learnt from MeyGen Phase 1a Part 2/3: Construction Phase. 2018.
33. Ofgem. Typical Domestic Consumption Values [Internet]. 2020 [cited 2019 Dec 9]. Available from: https://www.ofgem.gov.uk/gas/retail-market/monitoring-data-and-statistics/typical-domestic-consumption-values
34. Donovan C. MeyGen Section 36 Variation Report. 2018.
35. Goss Z, Piggot M, Kramer S, Avdis A, Angeloudis A, Cotter C. Competition effects between nearby tidal turbine arrays - optimal design for Alderney Race. In: Advances in Renewable Energies Offshore. Lisbon; 2018. p. 255–62.
36. Lewis M, Neill S, Robins P, Hashemi M. Resource assessment for futiue generations of tidal-stream energy arrays. Energy. 2015;83:403–15.
37. Funke S., Farrell P., Piggott M. Tidal turbine array optimisation using the adjoint approach. Renew Energy. 2014;63:658–73.

Tables

Table 1. Data inputs/modelling approach used in Cases 1-5. Case 1 is the approach taken in (5). Case 2-5 are undertaken in this work. Arrows indicate the data input/modelling approach that changes to go from the previous case to the next.

Case	1		2		3		4		5
Flow resolution	c. 10 km's	→	250 m		250 m		250 m		250 m
Array blockage	Excluded		Excluded	→	Included		Included		Included
Power coefficient	0.3		0.3		0.3	→	0.41		0.41
Array capacity	3.26 GW		3.26 GW		3.26 GW		3.26 GW	→	2.04 GW

Table 2. Specification of dual-rotor devices used in the small medium and large sub-arrays (5).

	Nominal depth	Hub height	Rotor diameter	Device rated speed		Device rated power	
				East Race	West Race	East Race	West Race
Small-rotor sub-arrays	28 m	14 m	14 m	4.0 m/s	2.5 m/s	3.05 MW	0.75 MW
Intermediate-rotor sub-arrays	36 m	20 m	19 m	4.1 m/s	2.6 m/s	6.20 MW	1.50 MW
Large-rotor sub-arrays	40 m	25 m	20.5 m	4.6 m/s	2.9 m/s	9.70 MW	2.40 MW

Table 3. Description of sub-arrays in the East and West Race. Each sub-array has 16 twin-rotor devices.

	Device rated power	**Sub-array power capacity**	**Number of sub-arrays**	**Total power capacity**
East Race				
Small-rotor sub-arrays	3.05 MW	49 MW	29	1421 MW
Intermediate-rotor sub-arrays	6.20 MW	99 MW	4	396 MW
Large-rotor sub-arrays	9.70 MW	155 MW	2	310 MW
Total			35	2127 MW
West Race				
Small-rotor sub-arrays	0.75 MW	12 MW	9	108 MW
Intermediate-rotor sub-arrays	1.50 MW	24 MW	19	456 MW
Large-rotor sub-arrays	2.40 MW	38 MW	15	570 MW
Total			43	1134 MW

Table 4. Case 2 estimated annual yield of sub-arrays within the Alderney Race. Numbers in brackets show results from Case 1 (5).

	Installed capacity	**Estimated Annual Energy**	**Capacity factor**
West Race			
Small-rotor sub-arrays	108 MW	0.37 TWh	39%
Intermediate-rotor sub-arrays	456 MW	1.29 TWh	32%
Large-rotor sub-arrays	570 MW	1.24 TWh	25%
Total	1135 MW	2.90 TWh (2.67 TWh)	29% (27%)
East Race			
Small-rotor sub-arrays	1421 MW	2.32 TWh	19%
Intermediate-rotor sub-arrays	396 MW	0.46 TWh	13%
Large-rotor sub-arrays	310 MW	0.28 TWh	10%
Total	2127 MW	3.06 TWh (4.73 TWh)	16% (25%)
Whole Race			
Total	3261 MW	5.96 TWh (7.40 TWh)	21% (26%)

Table 5. Case 3 estimated annual energy yield of sub-arrays within the Alderney Race, with consideration for blockage. Numbers in brackets show results for Case 2 (Section 3a), when array blockage is neglected.

	Installed Capacity	**Estimated Annual Energy**	**Capacity factor**
West Race			
Small sub-arrays	108 MW	0.21 TWh	22%
Medium sub-arrays	456 MW	0.46 TWh	12%
Large sub-arrays	570 MW	0.34 TWh	7%
Total	1135 MW	1.01 TWh (2.90 TWh)	10% (29%)
East Race			
Small sub-arrays	1421 MW	1.04 TWh	8%
Medium sub-arrays	396 MW	0.14 TWh	4%
Large sub-arrays	310 MW	0.11 TWh	4%
Total	2127 MW	1.29 TWh (3.06 TWh)	7% (16%)
Whole Race			
Total	3261 MW	2.30 TWh (5.96 TWh)	8% (21%)

Figures

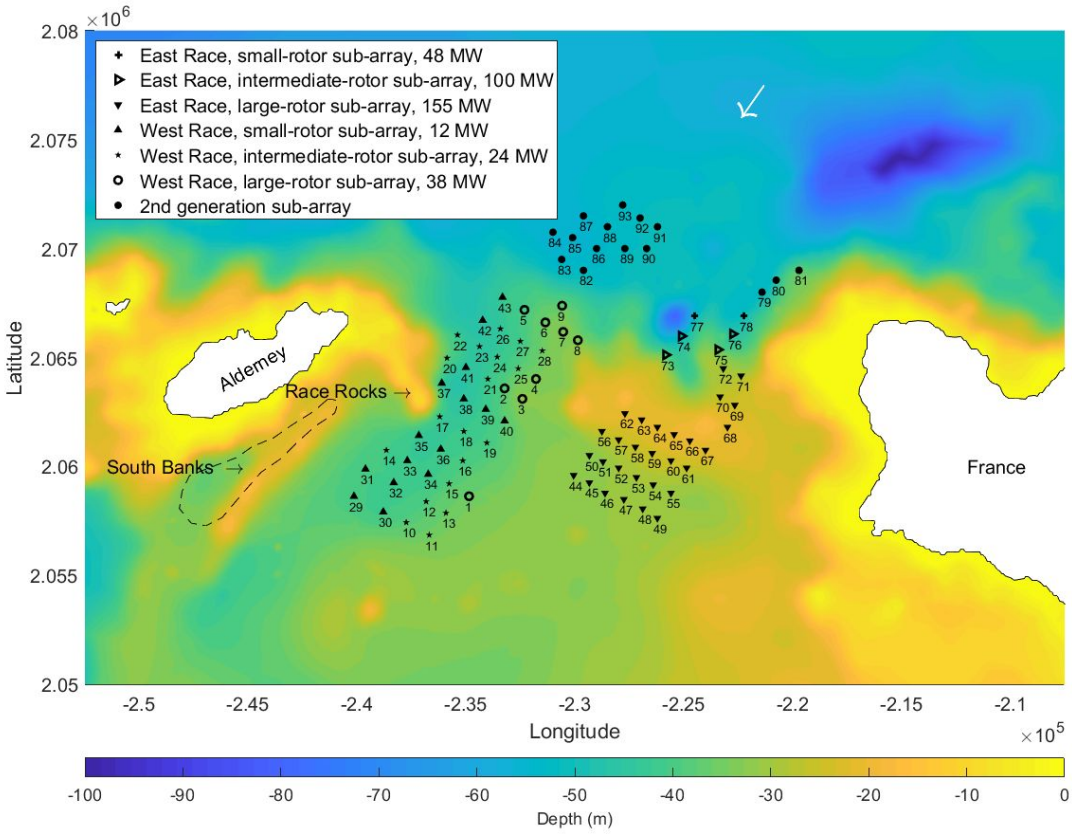

Figure 1. Layout of 1st and 2nd generation sub-arrays in the Alderney Race, first considered in (5). Depth contours are shown relative to Lowest Astronomical Tide (LAT). The location of Race Rocks and the South Banks are also shown. The arrow shows the direction of the dominant ebb tide.

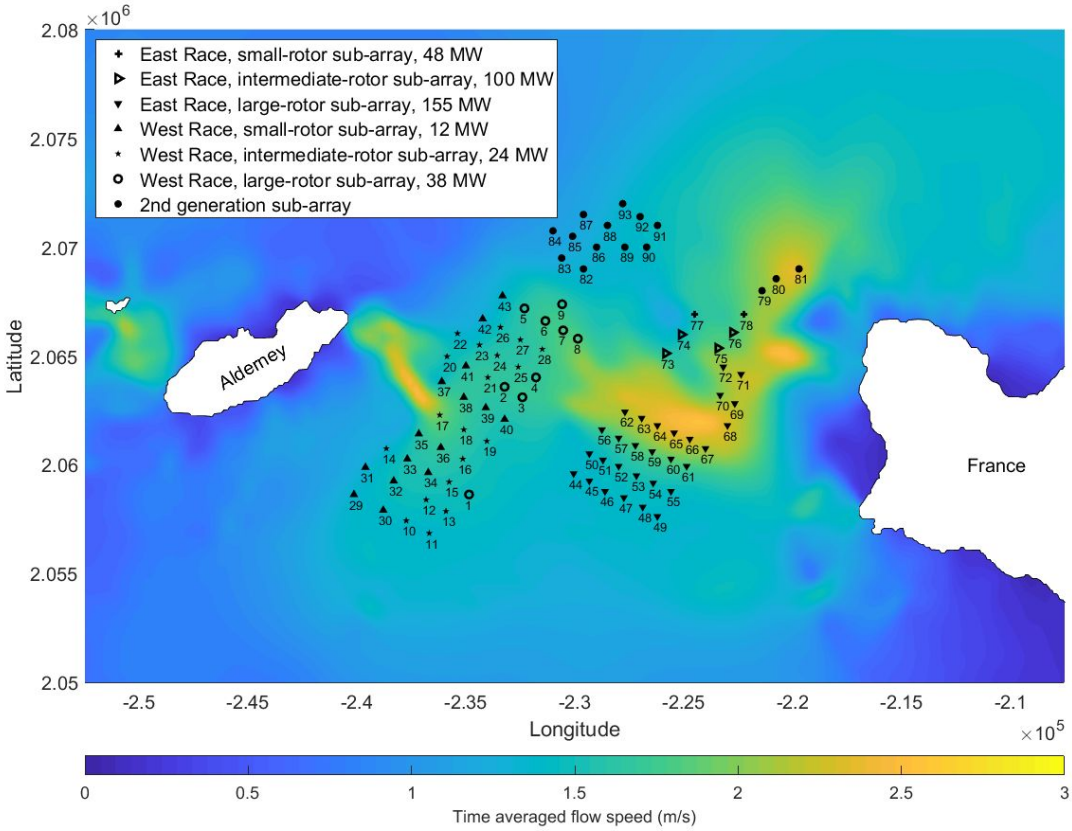

Figure 2. Time averaged ambient flow speed within the Alderney Race, with location of sub-arrays.

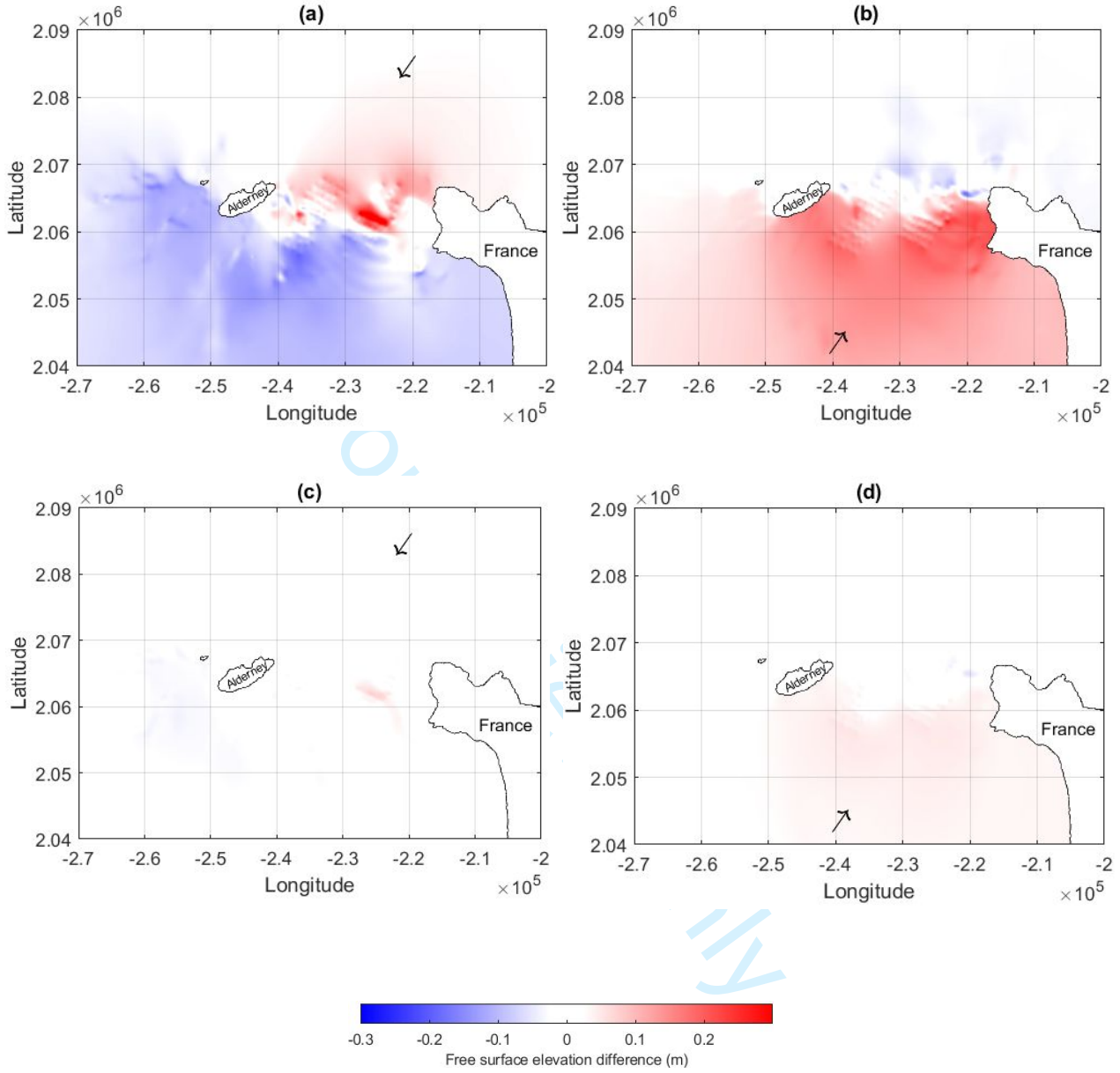

Figure 3. Free surface elevation difference between the ambient flow and flow with sub-array drag modelled during (a) peak spring ebb tide, (b) peak spring flood tide, (c) peak neap ebb tide and (d) peak neap flood tide. Arrows show the direction of the flow.

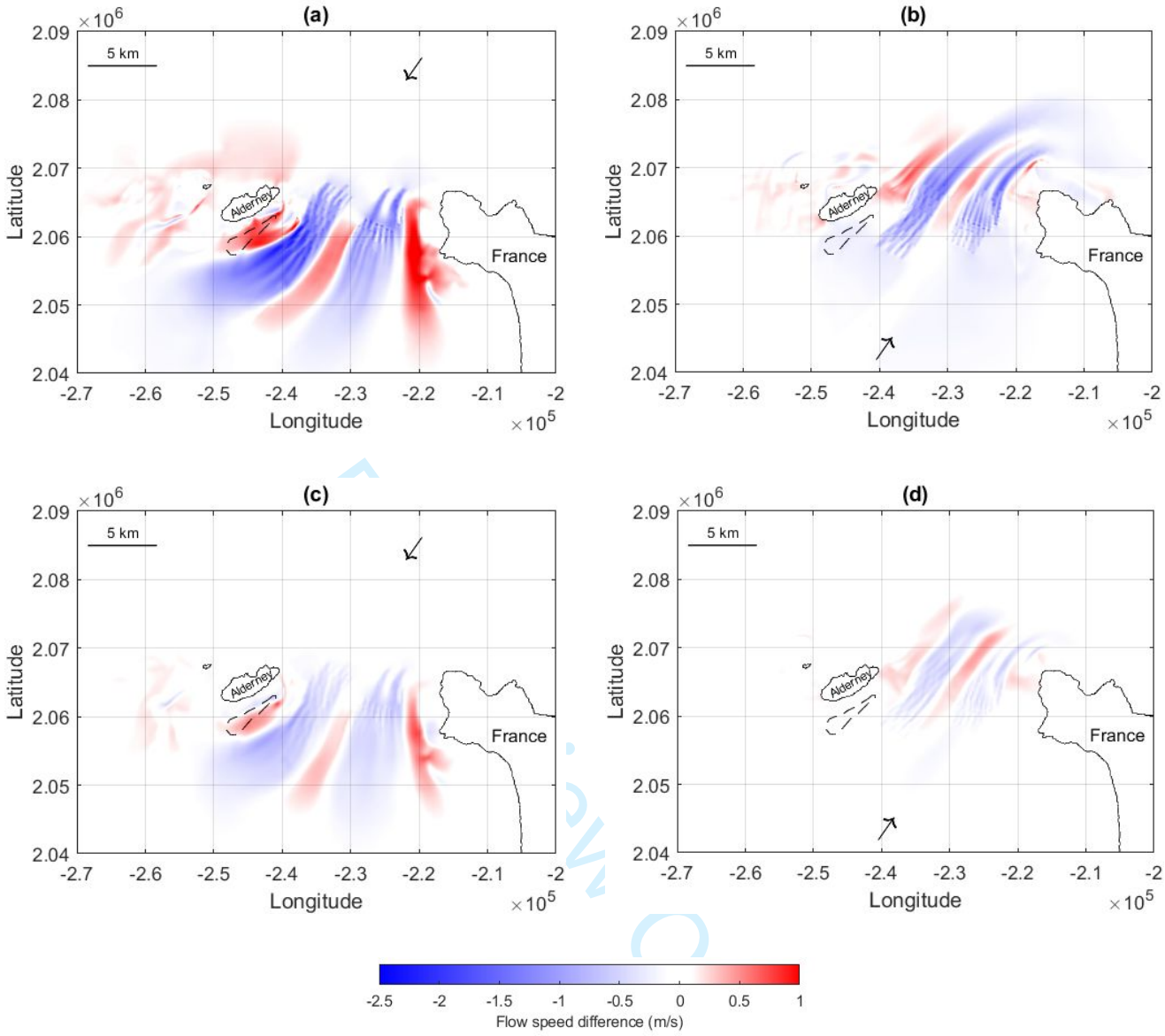

Figure 4. Time averaged flow speed difference between the ambient flow and flow with energy extraction modelled in the Alderney Race during (a) peak spring ebb tide, (b) peak spring flood tide, (c) peak neap ebb tide and (d) peak neap flood tide.

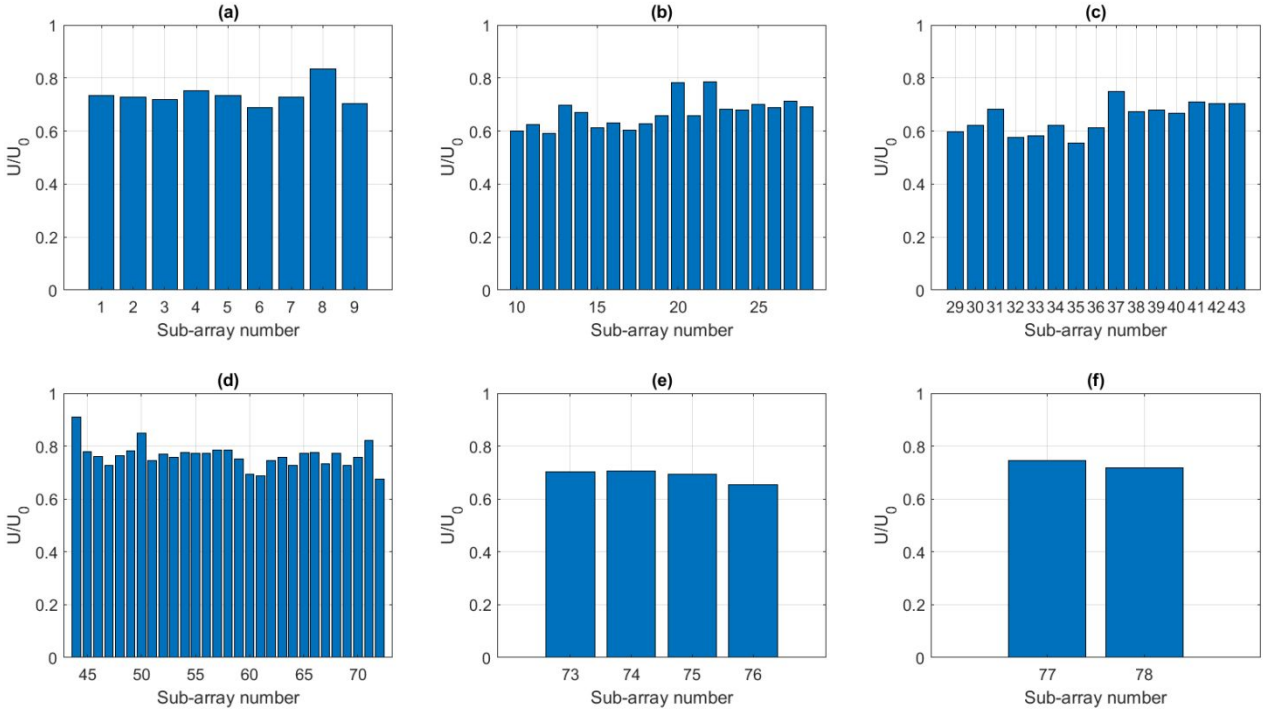

Figure 5. Ratio of time averaged flow speed to time averaged ambient flow speed at the location of the (a) West Race small-rotor sub-arrays, (b) West Race intermediate-rotor sub-arrays, (c) West Race large-rotor sub-arrays, (d) East Race small-rotor sub-arrays, (e) East Race intermediate-rotor sub-arrays, and (f) East Race Large-rotor sub-arrays.

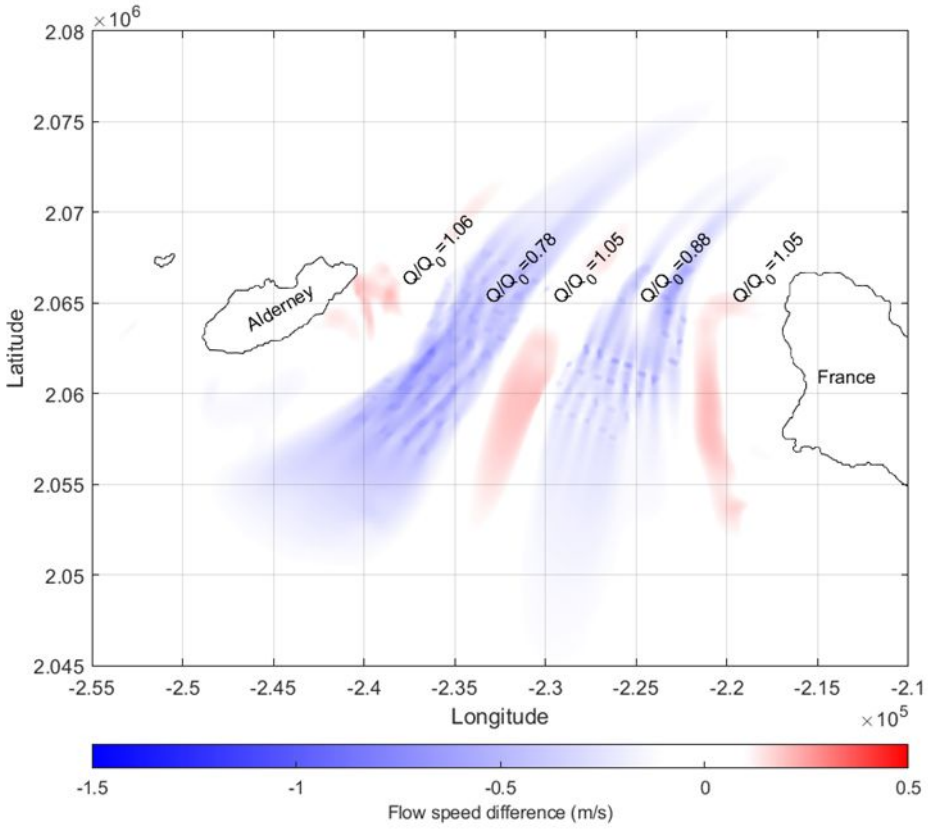

Figure 6. Contour plot showing the difference in flow speed, averaged over a spring neap period, with changes in the time averaged volume flux through the West flank, West Race sub-arrays, Central Flank, East Race sub-arrays and East flank also indicated.

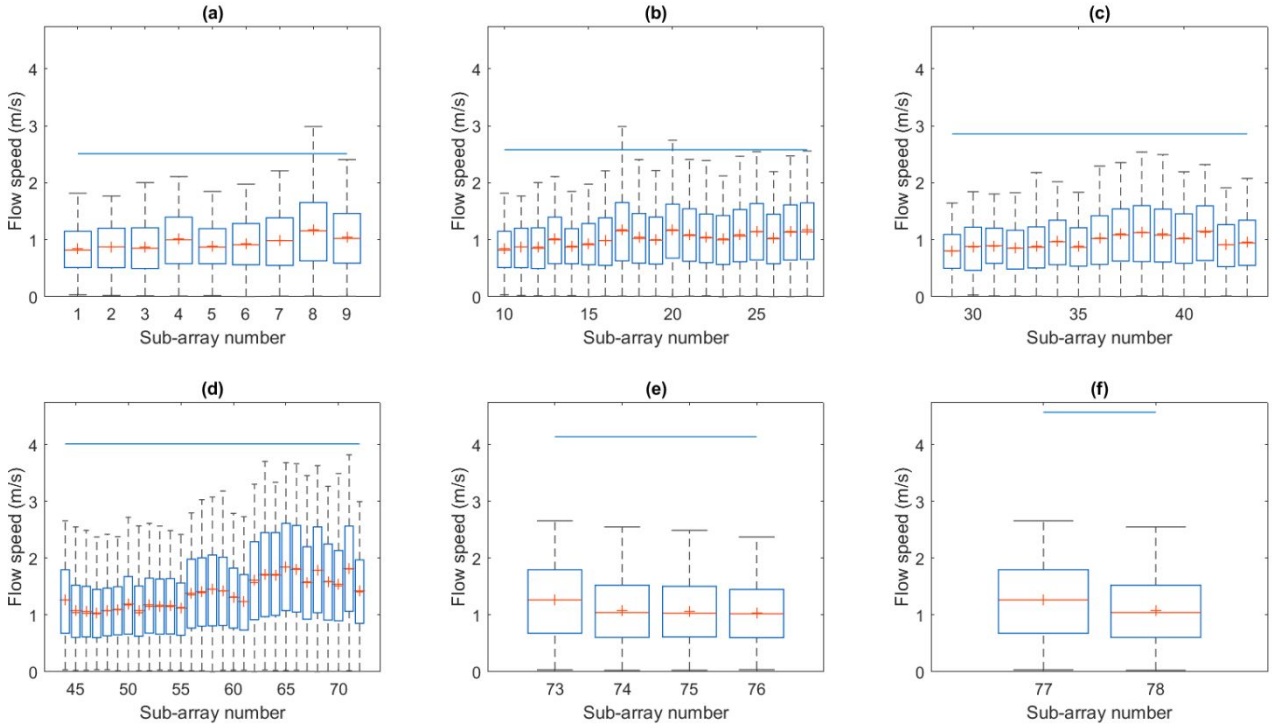

Figure 7. Box plots characterising the median flow speed (orange line), mean flow speed (orange cross), 25th percentile flow speed (lower edge of box), 75th percentile flow speed (upper edge of box), minimum flow speed (bottom bar), maximum flow speed (top bar and rated speed (blue line) at the location of the (a) West Race small-rotor sub-arrays, (b) West Race intermediate-rotor sub-arrays, (c) West Race large-rotor sub-arrays, (d) East Race small-rotor sub-arrays, (e) East Race intermediate-rotor sub-arrays, and (f) East Race Large-rotor sub-arrays.

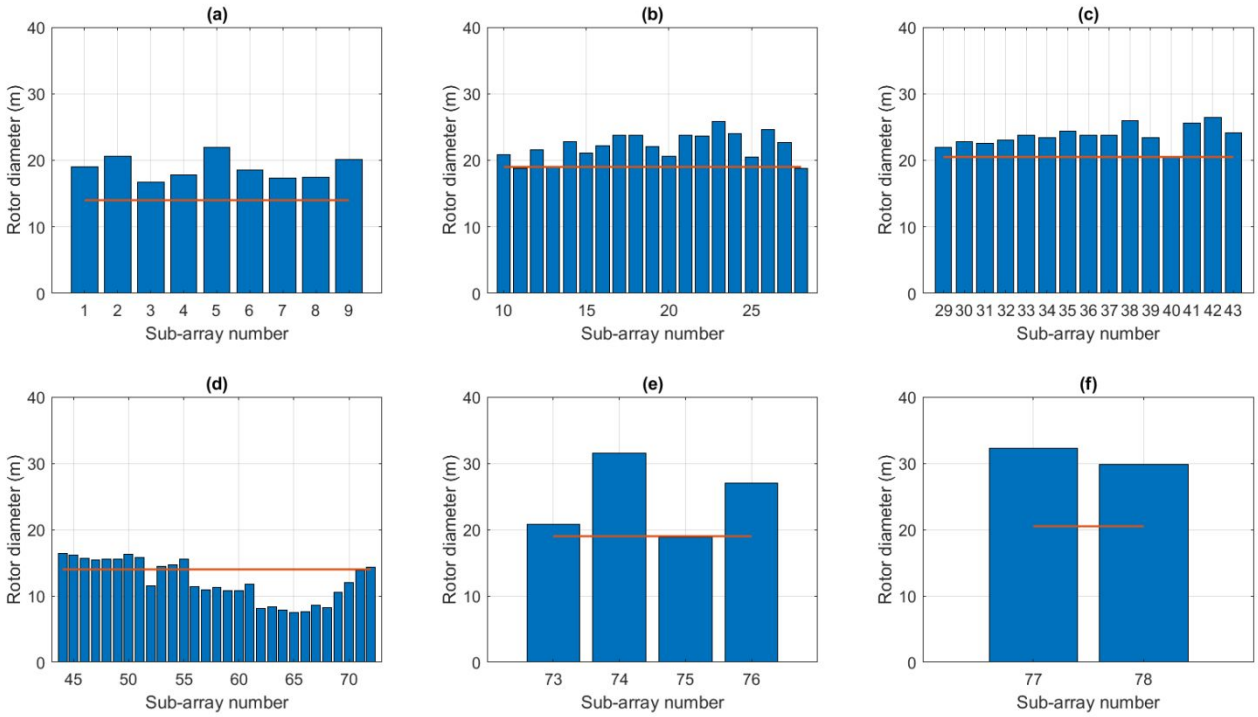

Figure 8. Maximum allowable rotor diameter of devices in the (a) West Race small-rotor sub-arrays, (b) West Race intermediate-rotor sub-arrays, (c) West Race large-rotor sub-arrays, (d) East Race small-rotor sub-arrays, (e) East Race intermediate-rotor sub-arrays, and (f) East Race Large-rotor sub-arrays. Orange lines shows the rotor diameter used to estimate energy yield in (5) and this paper.

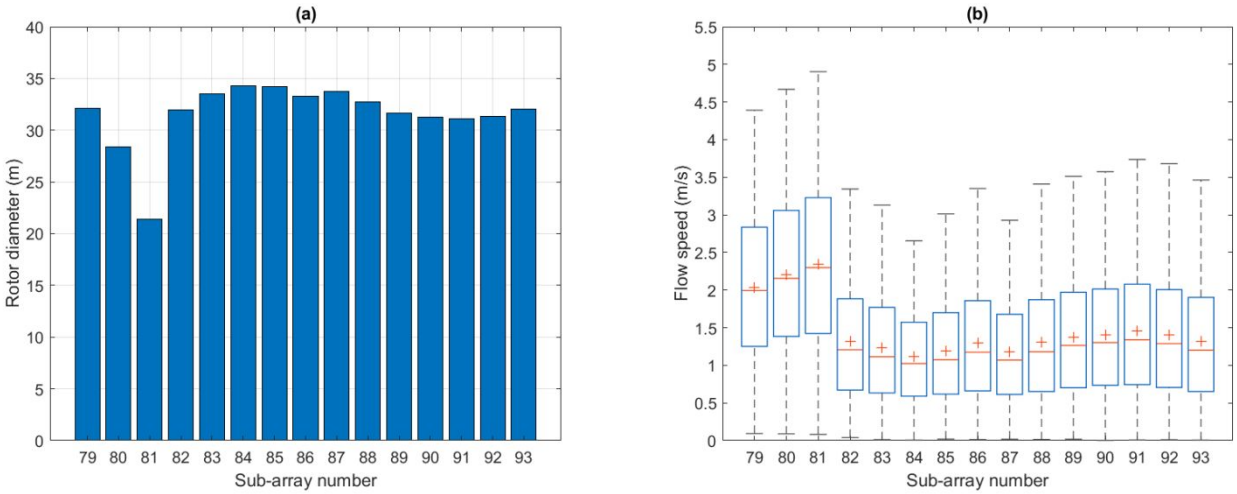

Figure 9. (a) Maximum allowable rotor diameter of devices in sub-arrays 79-93. (b) Box plot characterising median flow speed (orange line), mean flow speed (orange cross), 25th percentile flow speed (lower edge of box), 75th percentile flow speed (upper edge of box), minimum flow speed (bottom bar), maximum flow speed (top bar and rated speed (blue line) at sub-arrays 79-93, obtained from the ambient hydrodynamic model.

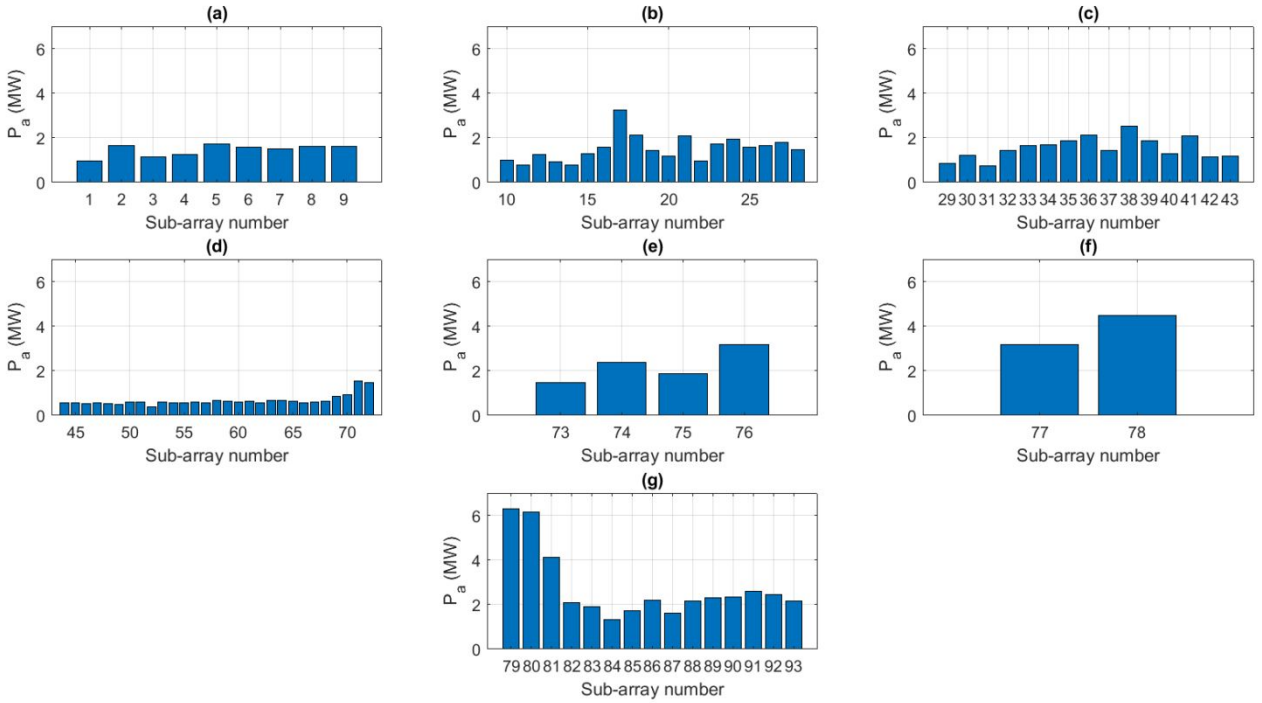

Figure 10. Time averaged available power based on the ambient flow at the location of the (a) West Race small-rotor sub-arrays, (b) West Race intermediate-rotor sub-arrays, (c) West Race large-rotor sub-arrays, (d) East Race small-rotor sub-arrays, (e) East Race intermediate-rotor sub-arrays, (f) East Race Large-rotor sub-arrays and (g) 2nd generation sub-arrays.

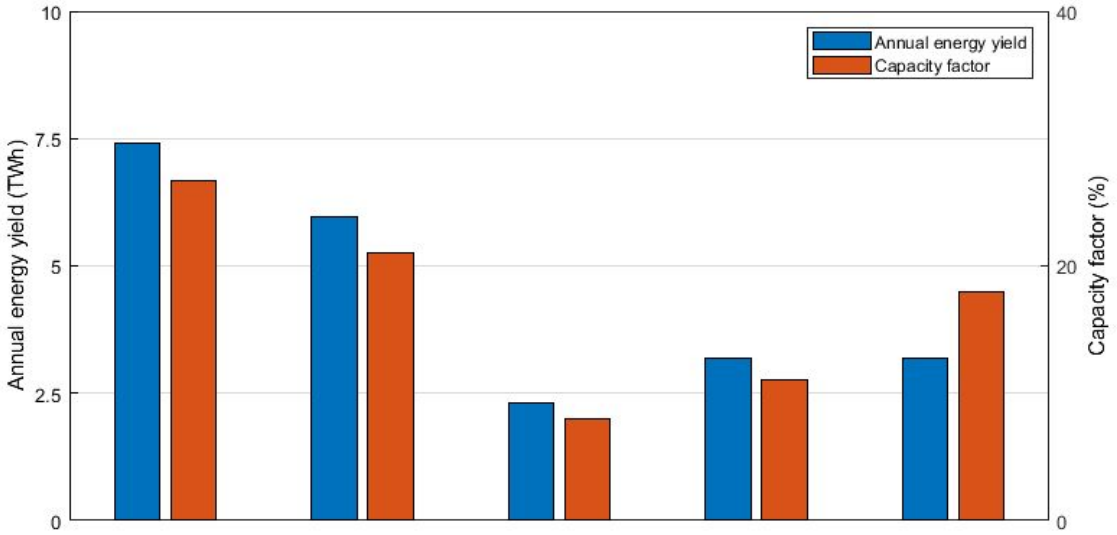

Case	1		2		3		4		5
Flow resolution	c. 10 km's	→	250 m		250 m		250 m		250 m
Array blockage	Excluded		Excluded	→	Included		Included		Included
Power coefficient	0.3		0.3		0.3	→	0.41		0.41
Array capacity	3.26 GW		3.26 GW		3.26 GW		3.26 GW	→	2.04 GW

Figure 11. Summary of modelling approach and estimated energy yield and capacity factor from the five energy yield assessment cases considered in this paper.

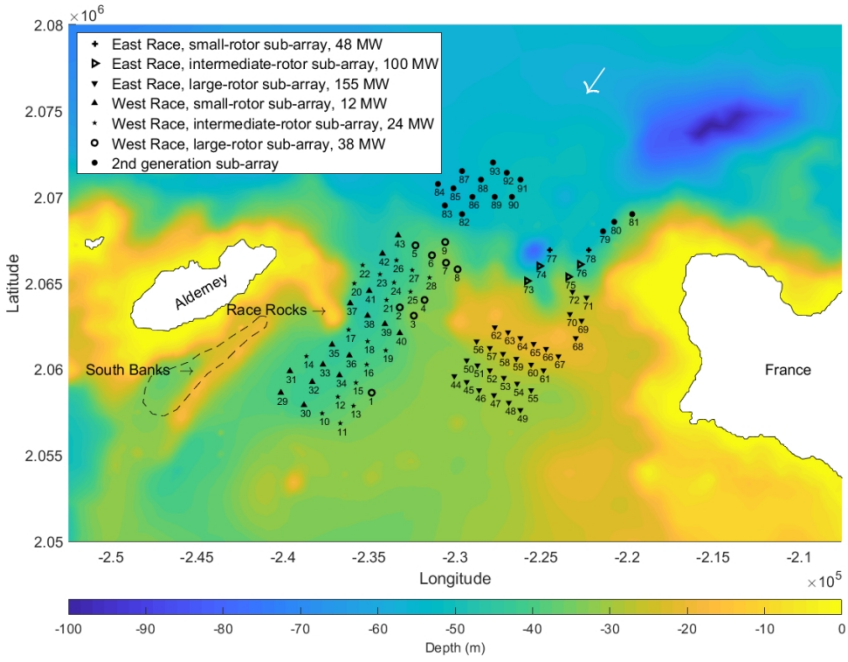

Layout of 1st and 2nd generation sub-arrays in the Alderney Race, first considered in (5). Depth contours are shown relative to Lowest Astronomical Tide (LAT). The location of Race Rocks and the South Banks are also shown. The arrow shows the direction of the dominant ebb tide.

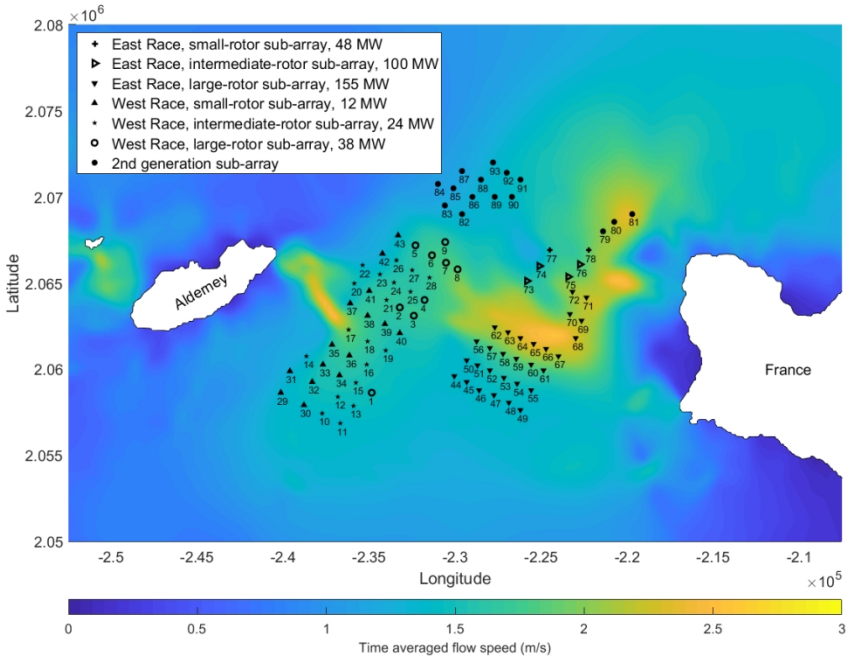

Time averaged ambient flow speed within the Alderney Race, with location of sub-arrays.

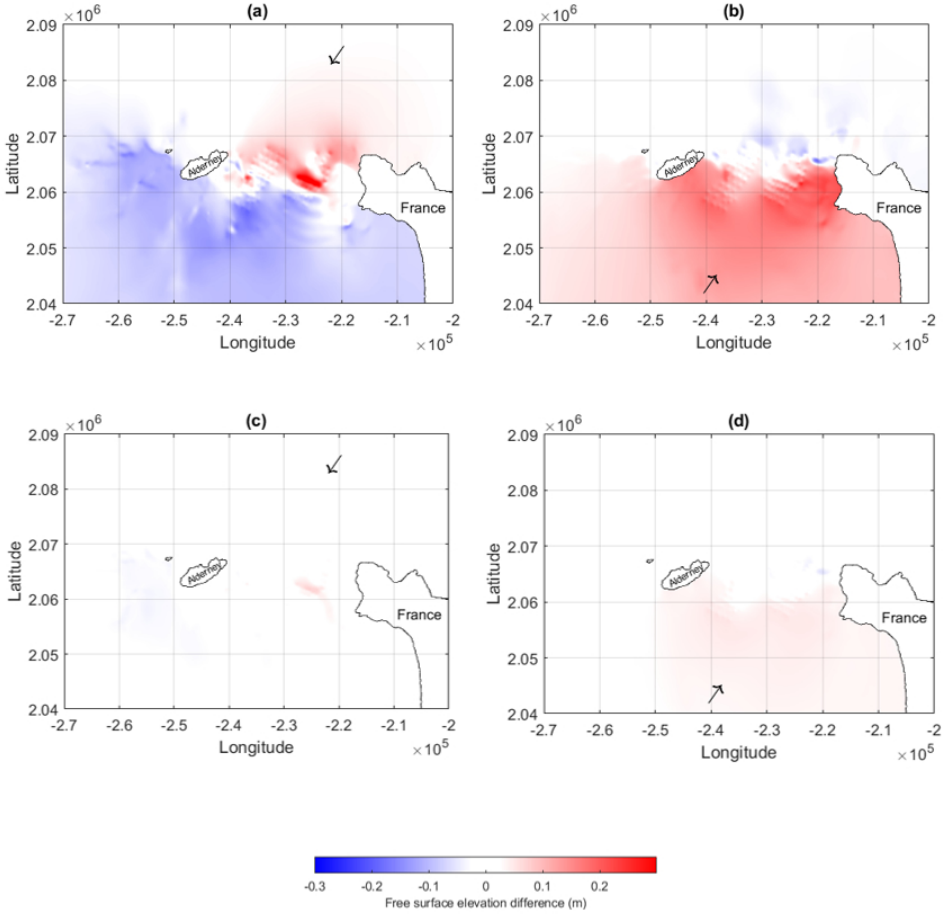

Free surface elevation difference between the ambient flow and flow with sub-array drag modelled during (a) peak spring ebb tide, (b) peak spring flood tide, (c) peak neap ebb tide and (d) peak neap flood tide. Arrows show the direction of the flow.

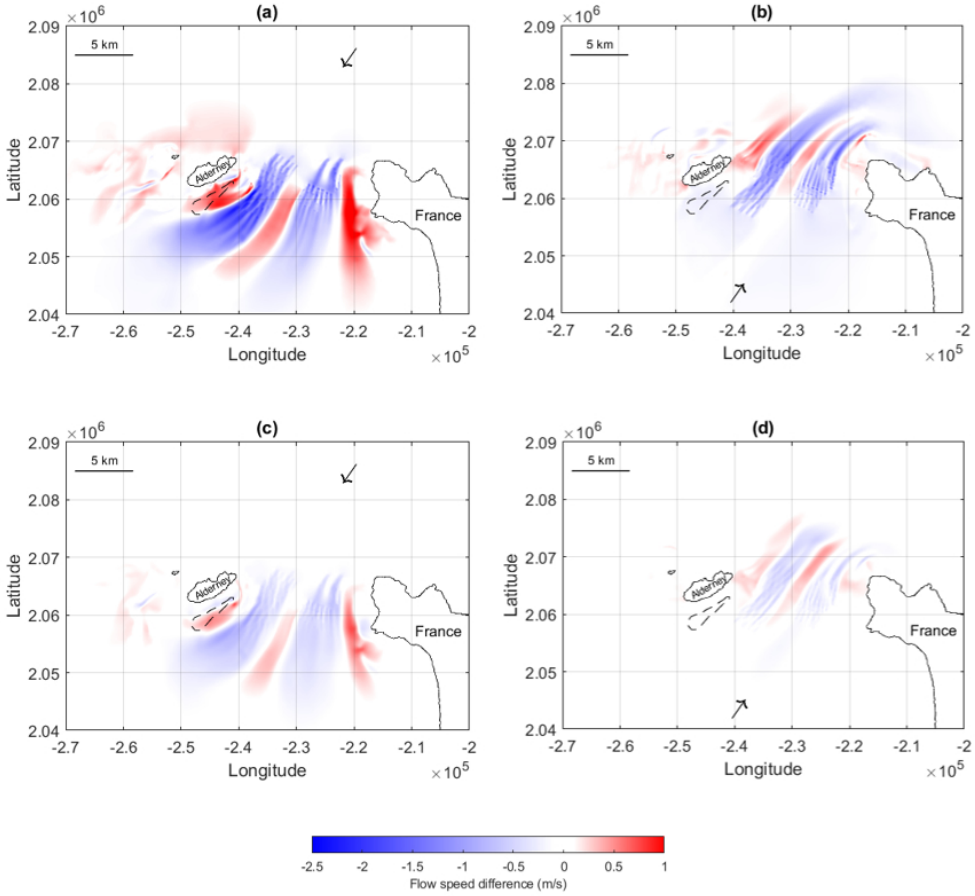

Time averaged flow speed difference between the ambient flow and flow with energy extraction modelled in the Alderney Race during (a) peak spring ebb tide, (b) peak spring flood tide, (c) peak neap ebb tide and (d) peak neap flood tide.

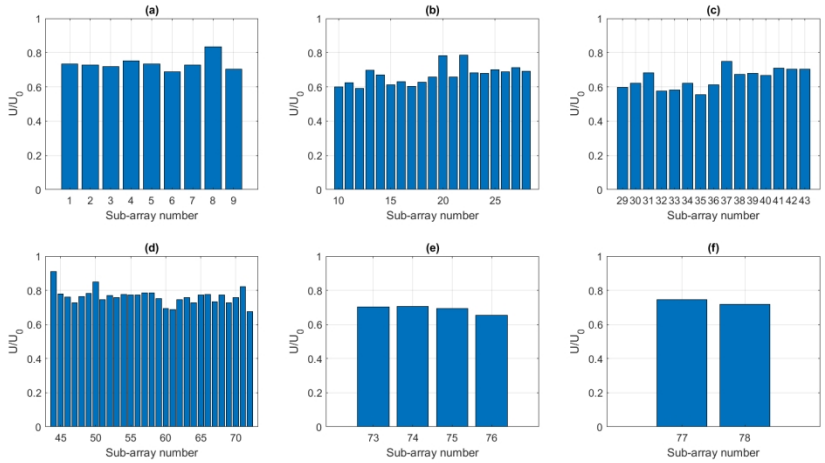

Ratio of time averaged flow speed to time averaged ambient flow speed at the location of the (a) West Race small-rotor sub-arrays, (b) West Race intermediate-rotor sub-arrays, (c) West Race large-rotor sub-arrays, (d) East Race small-rotor sub-arrays, (e) East Race intermediate-rotor sub-arrays, and (f) East Race Large-rotor sub-arrays.

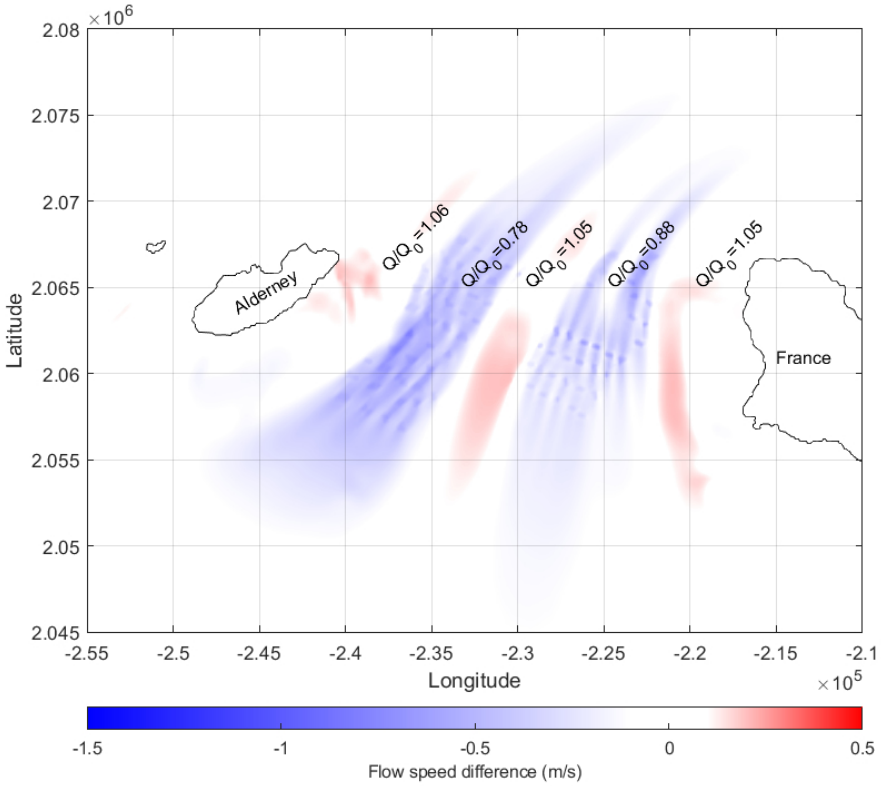

Contour plot showing the difference in flow speed, averaged over a spring neap period, with changes in the time averaged volume flux through the West flank, West Race sub-arrays, Central Flank, East Race sub-arrays and East flank also indicated.

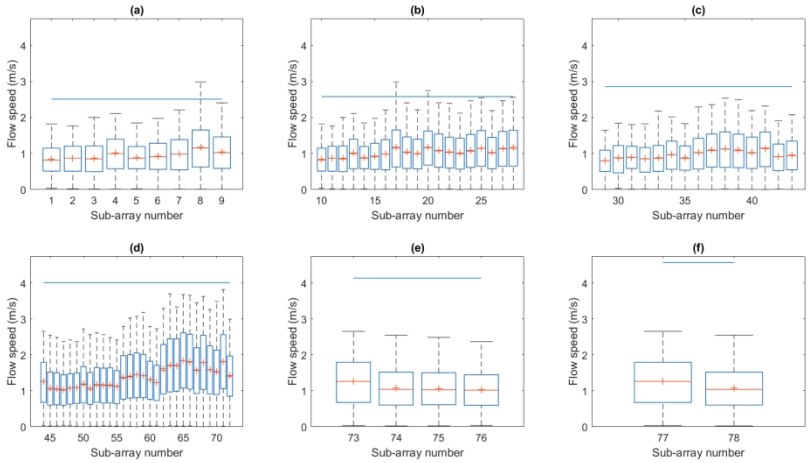

Box plots characterising the median flow speed (orange line), mean flow speed (orange cross), 25th percentile flow speed (lower edge of box), 75th percentile flow speed (upper edge of box), minimum flow speed (bottom bar), maximum flow speed (top bar and rated speed (blue line) at the location of the (a) West Race small-rotor sub-arrays, (b) West Race intermediate-rotor sub-arrays, (c) West Race large-rotor sub-arrays, (d) East Race small-rotor sub-arrays, (e) East Race intermediate-rotor sub-arrays, and (f) East Race Large-rotor sub-arrays.

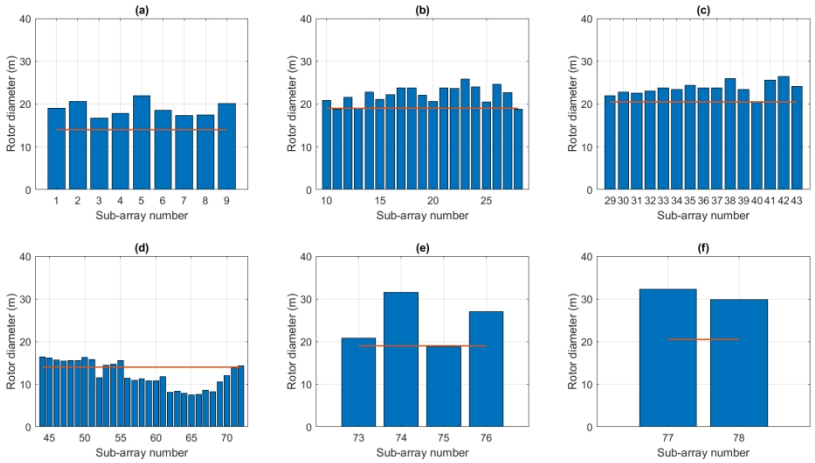

Maximum allowable rotor diameter of devices in the (a) West Race small-rotor sub-arrays, (b) West Race intermediate-rotor sub-arrays, (c) West Race large-rotor sub-arrays, (d) East Race small-rotor sub-arrays, (e) East Race intermediate-rotor sub-arrays, and (f) East Race Large-rotor sub-arrays. Orange lines shows the rotor diameter used to estimate energy yield in (5) and this paper.

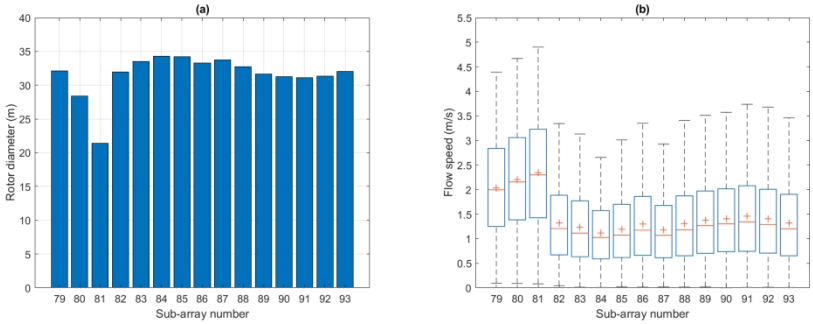

(a) Maximum allowable rotor diameter of devices in sub-arrays 79-93. (b) Box plot characterising median flow speed (orange line), mean flow speed (orange cross), 25th percentile flow speed (lower edge of box), 75th percentile flow speed (upper edge of box), minimum flow speed (bottom bar), maximum flow speed (top bar and rated speed (blue line) at sub-arrays 79-93, obtained from the ambient hydrodynamic model.

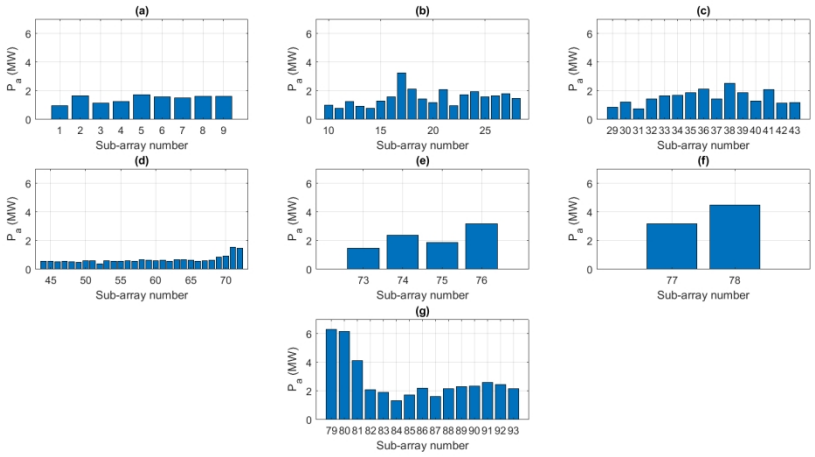

Time averaged available power based on the ambient flow at the location of the (a) West Race small-rotor sub-arrays, (b) West Race intermediate-rotor sub-arrays, (c) West Race large-rotor sub-arrays, (d) East Race small-rotor sub-arrays, (e) East Race intermediate-rotor sub-arrays, (f) East Race Large-rotor sub-arrays and (g) 2nd generation sub-arrays.

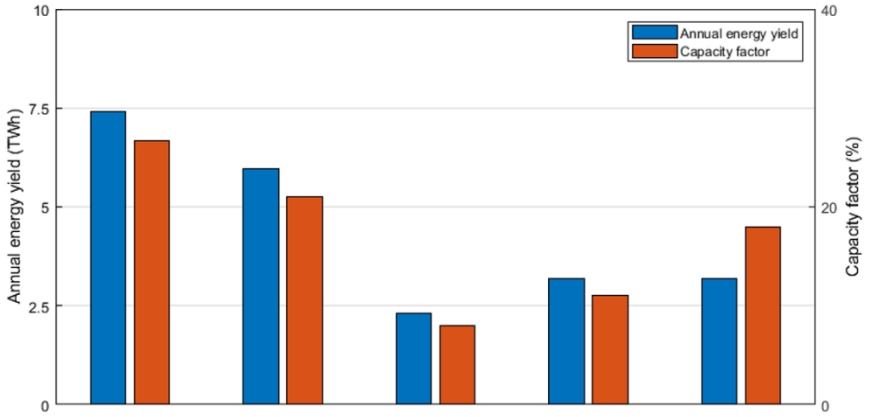

Case	1		2		3		4		5
Flow resolution	c. 10 km's	→	250 m		250 m		250 m		250 m
Array blockage	Excluded		Excluded	→	Included		Included		Included
Power coefficient	0.3		0.3		0.3	→	0.41		0.41
Array capacity	3.26 GW		3.26 GW		3.26 GW		3.26 GW	→	2.04 GW

Summary of modelling approach and estimated energy yield and capacity factor from the five energy yield assessment cases considered in this paper.